Supplemental Information for:

Mechanistic Insights into the Origin of Oxygen Migration Barrier

Daniele Vivona,[a] Kiarash Gordiz,[a] Randall Meyer,[b] Sumathy Raman,[b] and Yang Shao-Horn*[a,c,d]

[a] *Department of Mechanical Engineering, Massachusetts Institute of Technology, Cambridge, MA, USA.*

[b] *ExxonMobil Technology and Engineering Company, Annandale, NJ, USA.*

[c] *Department of Materials Science and Engineering, Massachusetts Institute of Technology, Cambridge, MA, USA.*

[d] *Research Laboratory of Electronics, Massachusetts Institute of Technology, Cambridge, MA, USA*

*Correspondence to: shaohorn@mit.edu

Contents:

Supplementary computational methods

Computation of vacancy formation energy

The NCC (V_O^x) and CC ($V_O^{\bullet\bullet}$) vacancy formation energies were computed based on the following expressions:[1]

$$E^f[V_O^x] = E_{tot}[V_O^x] - E_{perf} + E_{\frac{1}{2}O_2} + PA$$

$$E^f[V_O^{\bullet\bullet}] = E_{tot}[V_O^{\bullet\bullet}] - E_{perf} + E_{\frac{1}{2}O_2} + 2E_{F_{CC}} + PA$$

E^f is the vacancy formation energy, E_{tot} is the cohesive energy of the supercell, V_O^x is a neutral oxygen vacancy, and $V_O^{\bullet\bullet}$ corresponds to an oxygen vacancy created with a charge state of +2. $E_{\frac{1}{2}O_2}$ is half of the energy of an oxygen molecule at 0K calculated from DFT under our chosen formalism (see methods section), equal to -4.907 eV. $E_{F_{CC}}$ is the fermi energy computed in the defected structure with CC oxygen vacancies and is multiplied by 2 as two electrons were removed to introduce a charged (+2) oxygen vacancy. A potential alignment correction (PA) was also included[2,3] by aligning the core potential of electrons to correct for finite supercell effects.

Computation of vacancy excess charge density

The vacancy excess charge density was defined using a cluster-type approach based on Bader charge analysis.[4] To calculate the excess atomic charge for a specific site i ($q_{i,ex}$), we subtracted its Bader charge in the defected structure from its charge in the perfect structure, as shown in the equation:

$$q_{i,ex} = q_{i,defected} - q_{i,perfect}$$

In this equation, positive values of $q_{i,ex}$ indicate that site i has a higher electronic charge in the defected structure than in the perfect structure (more electronic charge has redistributed on site i upon vacancy formation). The vacancy excess charge $q_{V,ex}$ and vacancy volume V_V were computed by summing the atomic excess charges and volumes of all the first-shell neighbors of an oxygen vacancy. This first shell of neighbors included four A sites and two B sites for perovskite structures. When summing all the values of $q_{i,ex}$ for the first neighbors, positive resulting values of $q_{V,ex}$ indicate that electronic charge accumulates around the oxygen vacancy upon its formation.

$$q_{V,ex} = \sum_{\substack{\text{i=first neighbours} \\ \text{of the oxygen vacancy}}} q_{i,ex}$$

$$V_V = \sum_{\substack{\text{i=first neighbours} \\ \text{of the oxygen vacancy}}} V_i$$

Finally, we calculated the vacancy excess charge density $\rho_{V,ex}$ as the ratio between the vacancy excess charge and the vacancy volume:

$$\rho_{V,ex} = \frac{q_{V,ex}}{V_V}$$

The sign of $\rho_{V,ex}$ follows the same convention as $q_{V,ex}$ where positive values indicate that electronic charge accumulates around the oxygen vacancy upon its formation.

Supplementary Figures

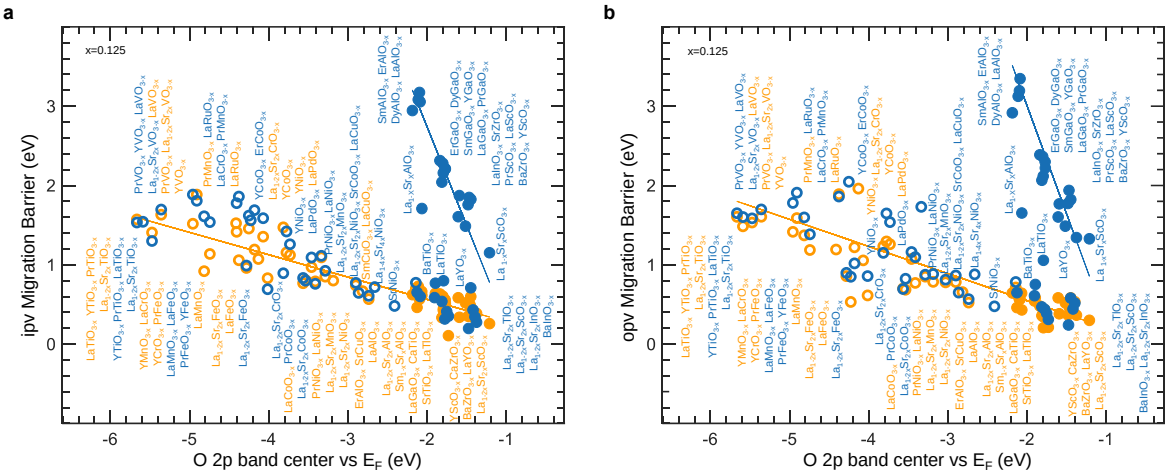

Figure S1. Comparison between ipv and opv migration barriers. Migration barrier computed for (a) ipv and (b) opv trajectories (in Figure 1b) in comparison with the energy of the O 2p band center vs. Fermi level descriptor computed on the perfect structure without oxygen vacancies.

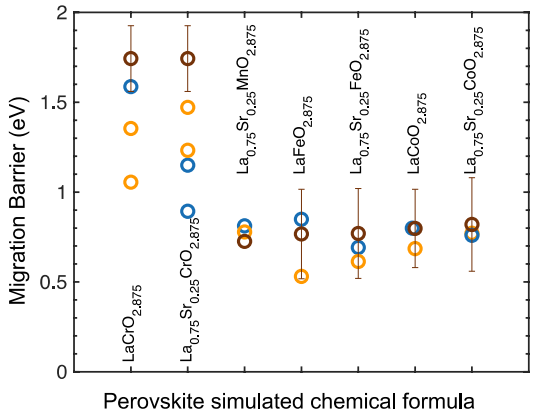

Figure S2. Comparison of computed and experimental data for perovskites with d electrons. Migration barriers as a function of the simulated chemical formula. Blue and orange circles represent NCC and CC migration barriers, respectively, while brown circles denote experimental data from the literature (tabulated in Table S4). $La_{0.75}Sr_{0.25}CoO_{2.875}$, $LaCoO_{2.875}$, $La_{0.75}Sr_{0.25}FeO_{2.875}$, $LaFeO_{2.875}$ were compared with $La_{0.75}Sr_{0.25}CoO_{3-x}$, $LaCoO_{3-x}$, $La_{0.9}Sr_{0.1}FeO_{3-x}$, $LaFeO_{3-x}$ from Ref.[5], $La_{0.75}Sr_{0.25}MnO_{2.875}$ was compared with $(La_{0.79}Sr_{0.20})MnO_{3-x}$ from Ref.[6], $La_{0.75}Sr_{0.25}CrO_{2.875}$ and $LaCrO_{2.875}$ were compared with $La_{0.9}Ca_{0.12}CrO_{3-x}$ from Ref.[7] Extracted migration barriers tabulated in Table S6.

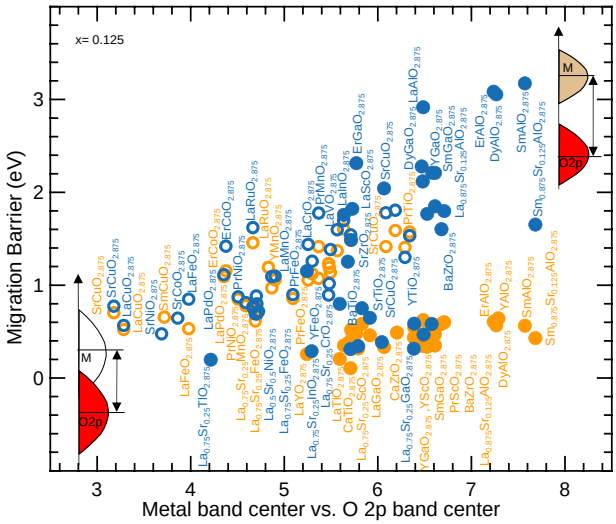

Figure S3. Correlation between migration barrier and covalency. Comparison between migration barrier and the energy of metal states vs. the O 2p band center (as depicted in the schematics).

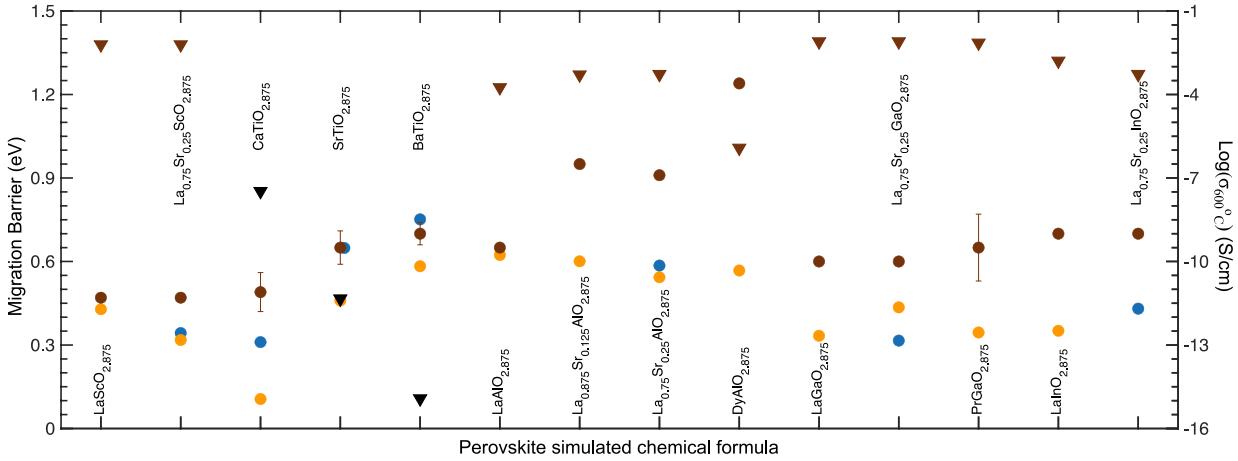

Figure S4. Comparison of computed and experimental data for perovskites without d electrons. Migration barriers as a function of the simulated chemical formula. Blue and orange circles represent NCC and CC migration barriers, respectively, while brown circles denote experimental data from the literature (tabulated in Table S4). $LaScO_{2.875}$ and $La_{0.75}Sr_{0.25}ScO_{2.875}$ were compared with $La_{0.9}Sr_{0.1}ScO_{3-x}$ from Ref.[8], $CaTiO_{2.875}$ was compared with $CaTiO_{3-x}$ from Ref.[5], $SrTiO_{2.875}$ was compared with $SrTiO_{3-x}$ from Ref.[9], $BaTiO_{2.875}$ was compared with $BaTiO_{3-x}$ from Ref.[10], $LaAlO_{2.875}$ was compared with $LaAlO_{3-x}$ cubic from Ref.[11], $La_{0.875}Sr_{0.125}Al_{2.875}$ was compared with $La_{0.9}Sr_{0.1}AlO_{3-x}$ from Ref.[12], $La_{0.75}Sr_{0.25}Al_{2.875}$ was compared with $La_{0.8}Sr_{0.2}AlO_{2.9}$ from Ref.[13], $DyAlO_{2.875}$ was compared with $Dy_{0.975}Ca_{0.025}AlO_{3-x}$ from Ref.[14], $LaGaO_{2.875}$ and $La_{0.75}Sr_{0.25}GaO_{2.875}$ were compared with $La_{0.9}Sr_{0.1}GaO_{3-x}$ from Ref.[12], $PrGaO_{2.875}$ was compared with $Pr_{0.93}Ca_{0.07}Ga_{0.85}Mg_{0.15}O_{3-x}$ from Ref.[15], $LaInO_{2.875}$ and $La_{0.75}Sr_{0.25}InO_{2.875}$ were compared with $La_{0.9}Sr_{0.1}InO_{3-x}$ from Ref.[12] Extracted migration barriers tabulated in Table S6. Brown (black) Triangles correspond to the values of conductivity (diffusivity measured in m^2/s) extracted at 600 °C from the same references.

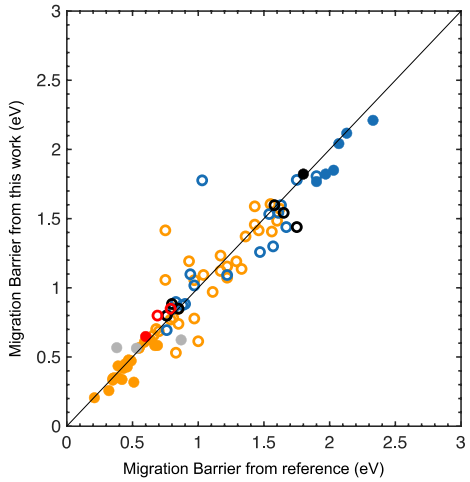

Figure S5. Comparison between migration barriers in this work and computational literature. Empty and solid circles correspond to oxides with and without d electrons, respectively. Orange data points correspond to CC migration barriers from this work compared to those reported in Ref.[16]. Blue datapoints correspond to NCC migration barriers from this work compared to those reported in Ref.[16]. Black datapoints correspond to NCC migration barriers compared to those reported in Ref.[17], and gray datapoints correspond to CC migration barriers compared to those reported in Ref.[14]. Data extracted from literature are tabulated in Table S7.

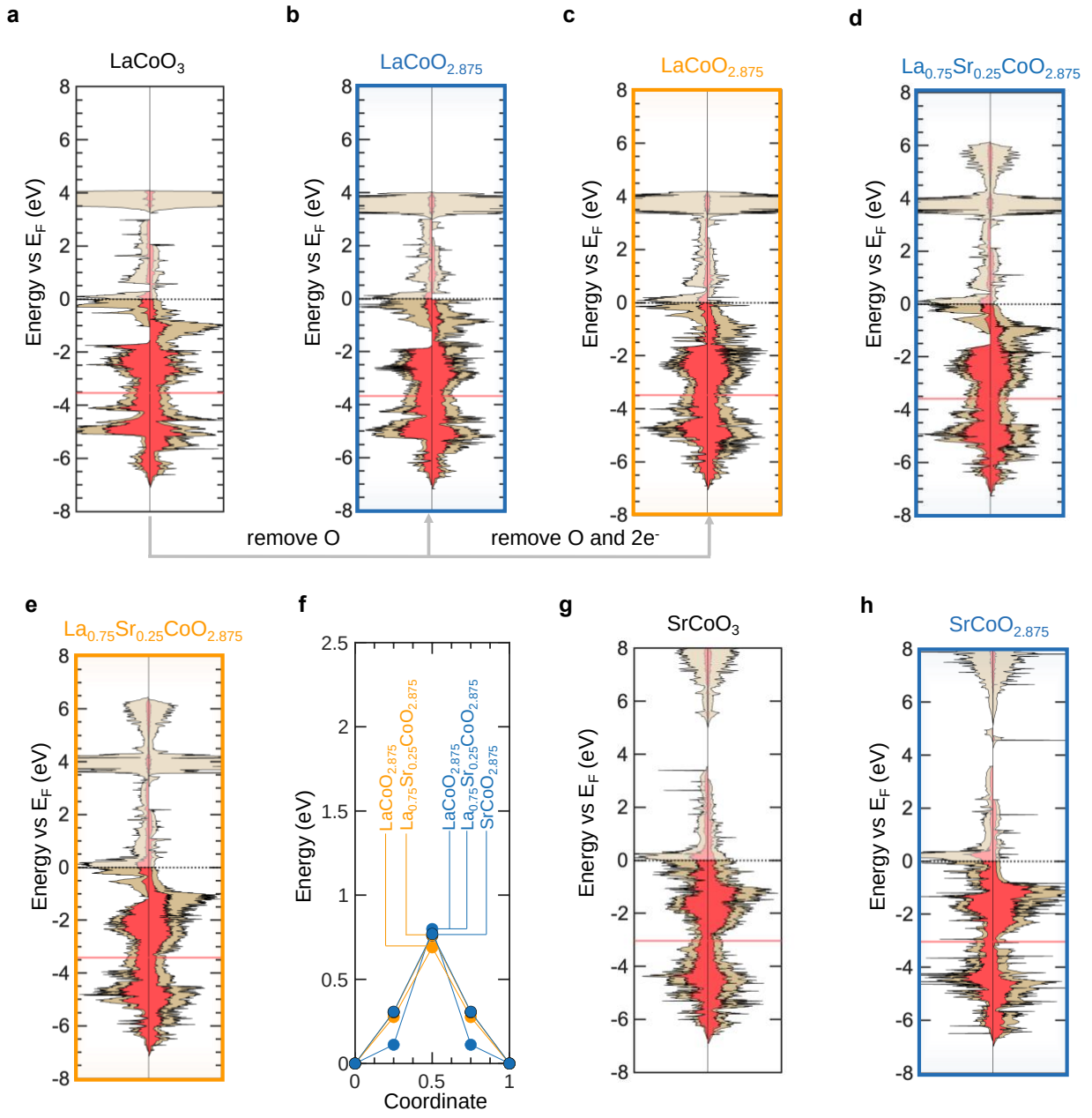

Figure S6. Electronic signatures of oxygen vacancies and migration barriers in (La,Sr)CoO_{3-x}. Computed electronic density of states (DOS) of (a) $LaCoO_3$, $LaCoO_{2.875}$ with (b) NCC and (c) CC oxygen vacancies, and $La_{0.75}Sr_{0.25}CoO_{2.875}$ with (d) NCC and (e) CC oxygen vacancies. (f) NCC (blue) and CC (orange) energy landscapes of (La,Sr)CoO_{3-x}. Computed electronic DOS of (g) $SrCoO_3$, and (h) $SrCoO_{2.875}$ with NCC oxygen vacancies.

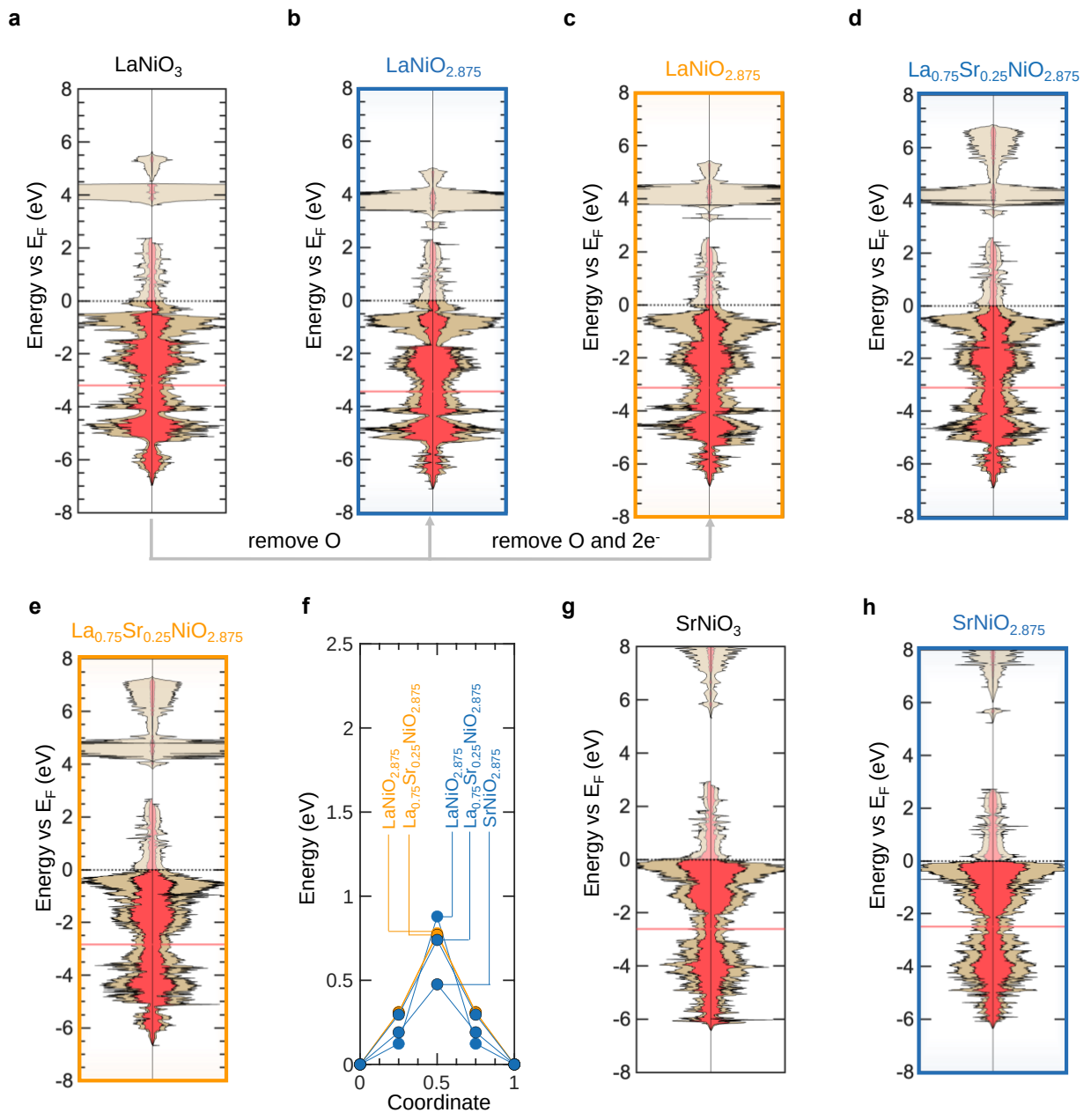

Figure S7. Electronic signatures of oxygen vacancies and migration barriers in (La,Sr)NiO_{3-x}.. Computed electronic DOS of (a) $LaNiO_3$, $LaNiO_{2.875}$ with (b) NCC and (c) CC oxygen vacancies, and $La_{0.75}Sr_{0.25}NiO_{2.875}$ with (d) NCC and (e) CC oxygen vacancies. (f) NCC (blue) and CC (orange) energy landscapes of (La,Sr)NiO_{3-x}. Computed electronic DOS of (g) $SrNiO_3$, and (h) $SrTiO_{2.875}$ with NCC oxygen vacancies.

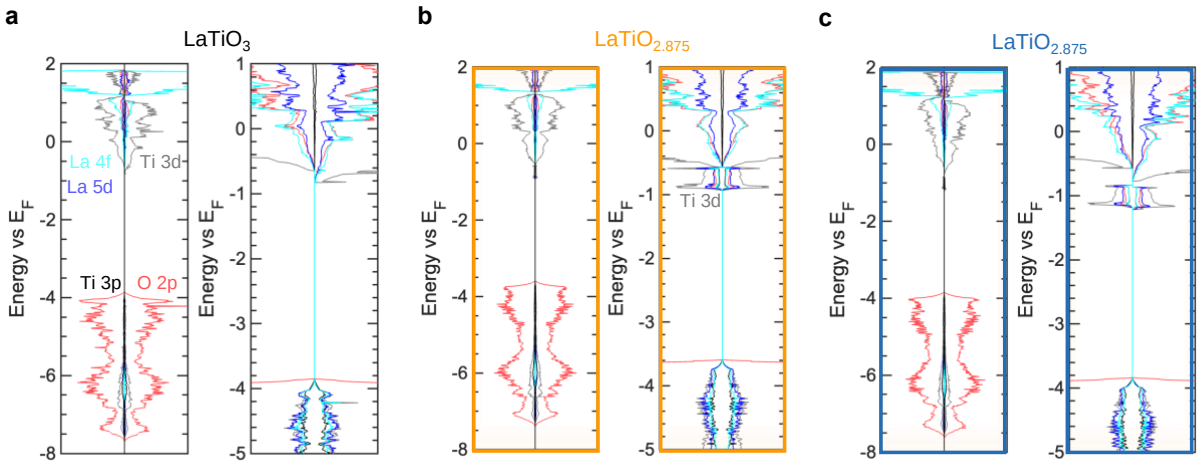

Figure S8. Origin of vacancy electronic states in $LaTiO_{2.875}$. Orbital-projected DOS of (a) $LaTiO_3$ (b) CC $LaTiO_{2.875}$, and (c) NCC $LaTiO_{2.875}$. Electronic orbitals are visualized in different colors as indicated in panel (a): cyan for La 4f, blue for La 5d, gray for Ti 3d, black for Ti 3p, and red for O 2p. For each panel, a zoomed version of the plot (between -5 and 1 eV) is included on the right.

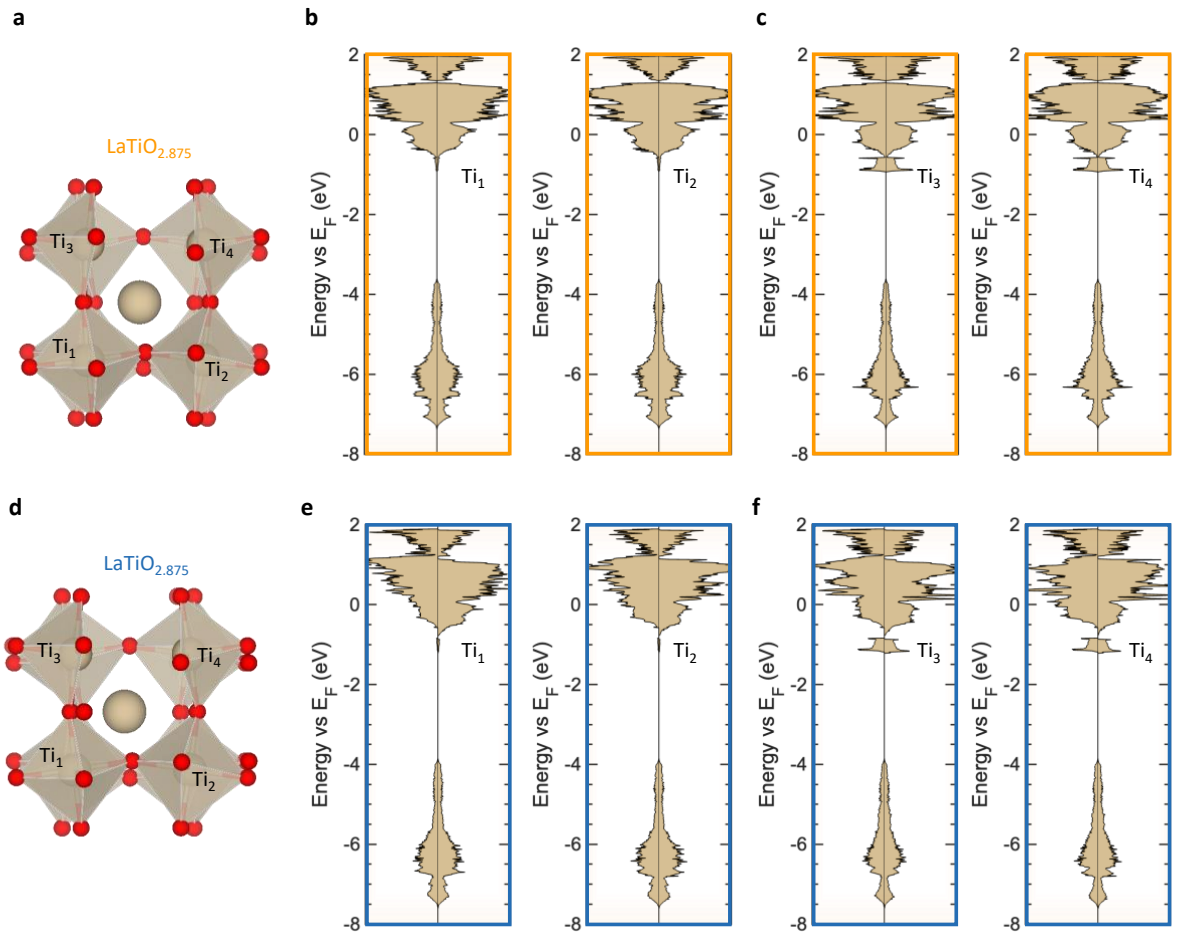

Figure S9. Site-projected DOS of $LaTiO_{2.875}$. (a) CC defected supercell of $LaTiO_{2.875}$. Four B-site Ti ions are labeled. Ti_1 and Ti_2 are not neighbors to the oxygen vacancy while Ti_3 and Ti_4 are neighbors to the oxygen vacancy. (b) Computed DOS of CC $LaTiO_{2.875}$ projected on (b) not neighbors to the vacancy Ti_1 (left) and Ti_2 (right) and (c) neighbors to the vacancy Ti_3 (left) and Ti_4 (right). (d) NCC defected supercell of $LaTiO_{2.875}$. and DOS of NCC $LaTiO_{2.875}$ projected on (e) not neighbors to the vacancy and (f) neighbors to the vacancy.

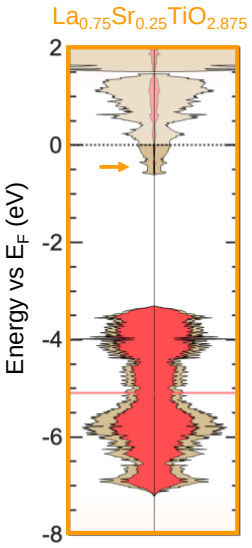

Figure S10. Electronic DOS of $La_{0.75}Sr_{0.25}TiO_{2.875}$ with CC oxygen vacancies.

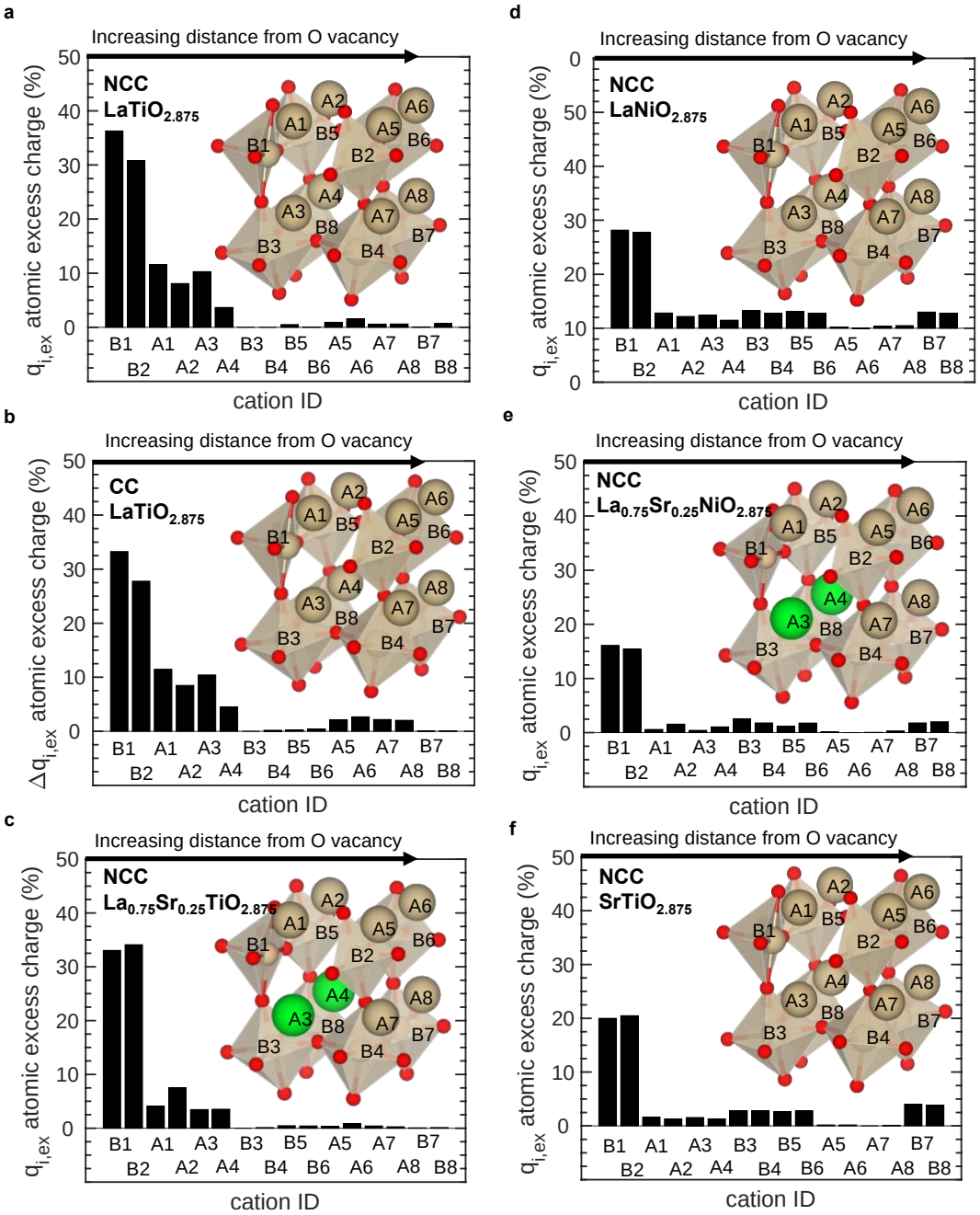

Figure S11. Trends in excess charge screening of oxygen vacancies. Normalized atomic excess charge density distribution on the cation sublattice, sorted by distance from the oxygen vacancy, for (a) NCC $LaTiO_{2.875}$ (b) CC $LaTiO_{2.875}$, NCC (c) $La_{0.75}Sr_{0.25}TiO_{2.875}$, (d) NCC $LaNiO_{2.875}$, (e) NCC $La_{0.75}Sr_{0.25}NiO_{2.875}$, and (f) NCC $SrTiO_{2.875}$. Values of atomic excess charges $q_{i,ex}$ were normalized based on the total charge for easier comparison. For CC, the atomic excess charges $\Delta q_{i,ex}$ were referenced to their minimum. Schematic structures with cation IDs corresponding to the x-axis are added to each panel with substituent atoms highlighted in green.

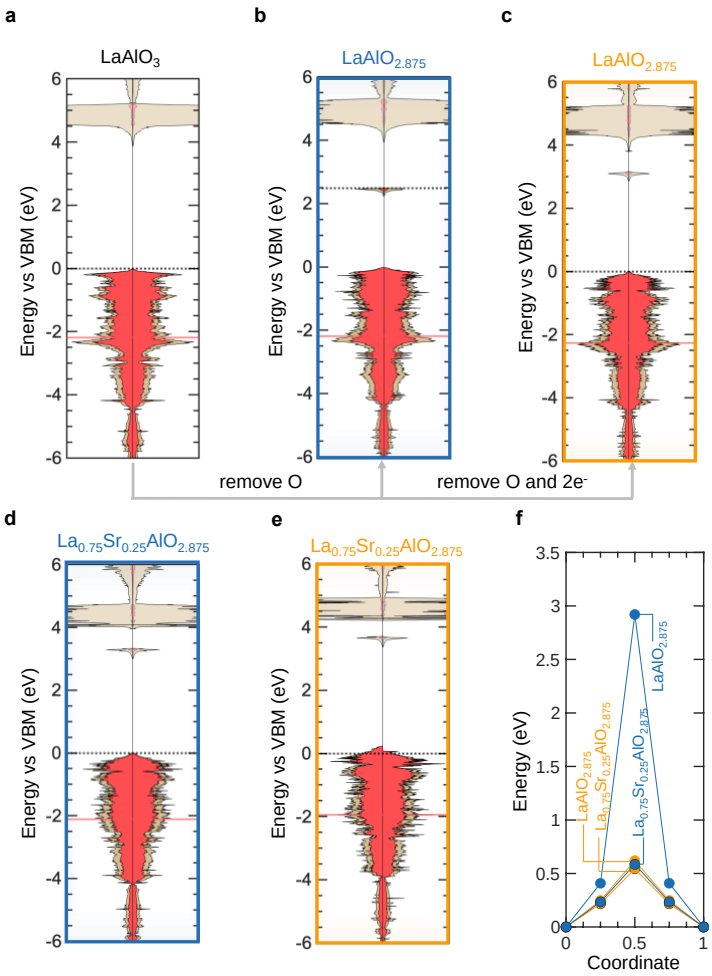

Figure S12. Electronic signatures of oxygen vacancies and migration barriers in (La,Sr)AlO_{3-x}. Computed electronic DOS of (a) $LaAlO_3$, $LaAlO_{2.875}$ with (b) NCC and (c) CC oxygen vacancies, and $La_{0.75}Sr_{0.25}AlO_{2.875}$ with (d) NCC and (e) oxygen vacancies. The DOS is referenced to the valence band maximum (VBM) of the perfect structure ($LaAlO_3$). (f) NCC (blue) and CC (orange) energy landscapes of (La,Sr)AlO_{3-x}.

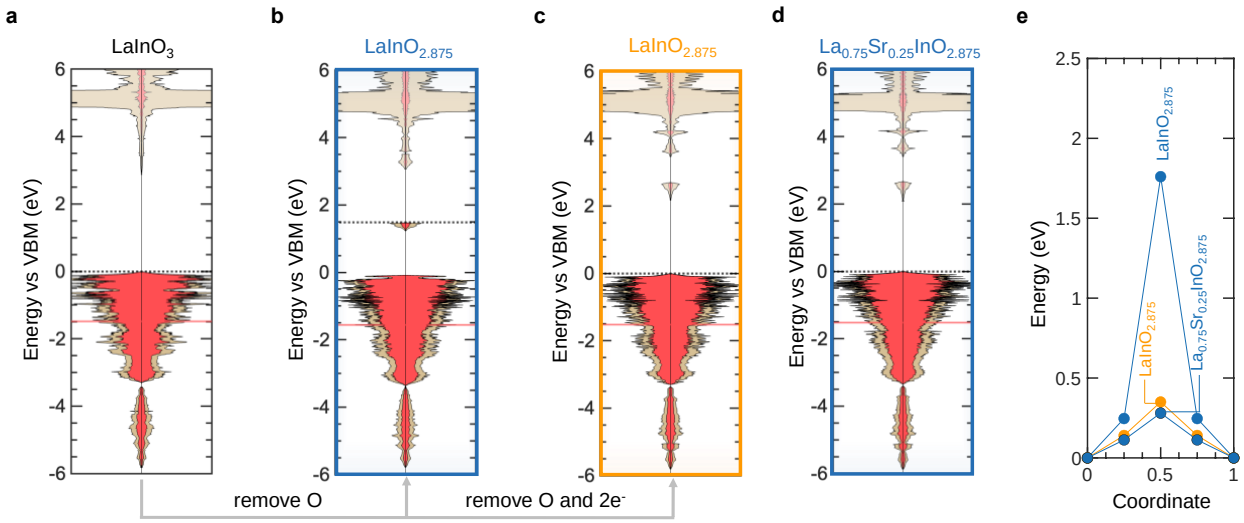

Figure S13. Electronic signatures of oxygen vacancies and migration barriers in (La,Sr)InO_{3-x}. Computed electronic DOS of (a) $LaInO_3$, $LaInO_{2.875}$ with (b) NCC and (c) CC oxygen vacancies, and $La_{0.75}Sr_{0.25}InO_{2.875}$ with (d) NCC and (e) oxygen vacancies. (f) NCC (blue) and CC (orange) migration barrier of (La,Sr) InO_{3-x}.

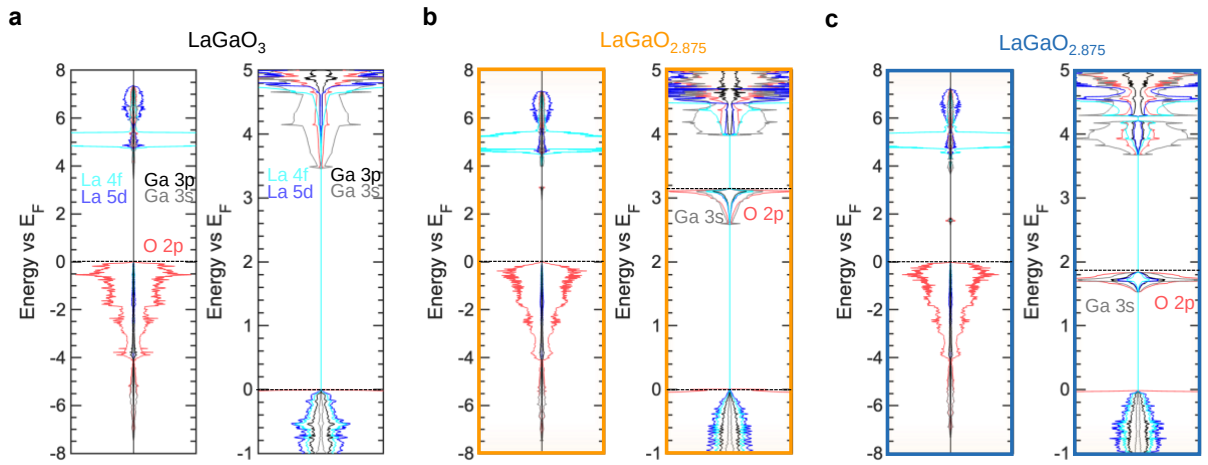

Figure S14. Origin of vacancy electronic states in $LaGaO_{2.875}$. Orbital-projected DOS of (a) $LaGaO_3$ (b) CC $LaGaO_{2.875}$, and (c) NCC $LaGaO_{2.875}$. Electronic orbitals are visualized in different colors as indicated in panel (a): cyan for La 4f, blue for La 5d, gray for Ga 3s, black for Ga 3p, and red for O 2p. For each panel a zoomed version of the plot (between -1 and 5 eV) is included on the right. The O 2p DOS is collapsed as a straight horizontal line in the zoomed version (right panels) of the plots.

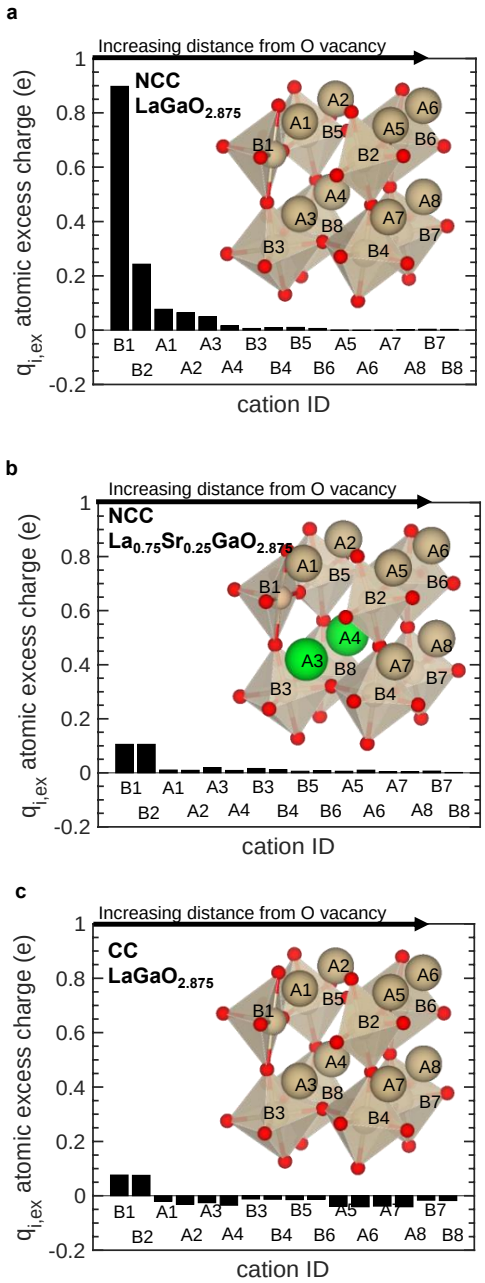

Figure S15. Charge localization in oxygen vacancies of (La,Sr)$GaO_{2.875}$. Atomic excess charge density distribution on the cation sublattice sorted by distance from the oxygen vacancy for (a) NCC $LaGaO_{2.875}$ (b) NCC $La_{0.75}Sr_{0.25}GaO_{2.875}$, and c) CC $LaGaO_{2.875}$. A schematic structure with cations IDs corresponding to the x-axis is added in each panel. Substituent atoms are indicated in green. It is seen that Sr-substitution (panel b) prevents accumulation of localized charge near oxygen vacancy, similar to CC $LaGaO_{2.875}$ (panel c). The atomic excess charge is evaluated as described in the supplementary computational methods.

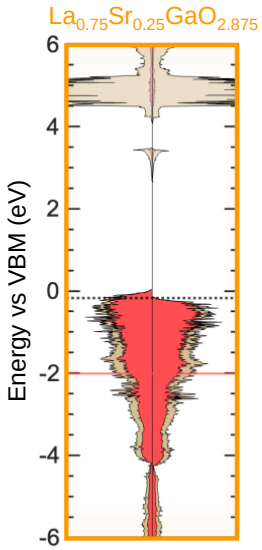

Figure S16. Electronic DOS of $La_{0.75}Sr_{0.25}GaO_{2.875}$ with NCC oxygen vacancies.

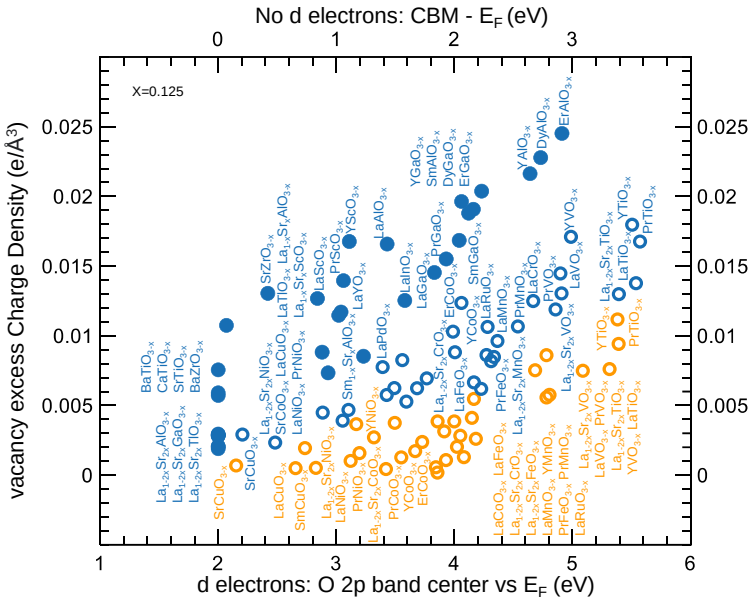

Figure S17. Electronic descriptors of vacancy excess charge density. Bottom x-axis for oxides with d electrons: comparison between the vacancy excess charge density and the O 2p band center vs. Fermi level (E_F). Top x-axis for oxides without d electrons: comparison between the vacancy excess charge density and the energy of lowest unoccupied vs. highest occupied states for oxides without d electrons.

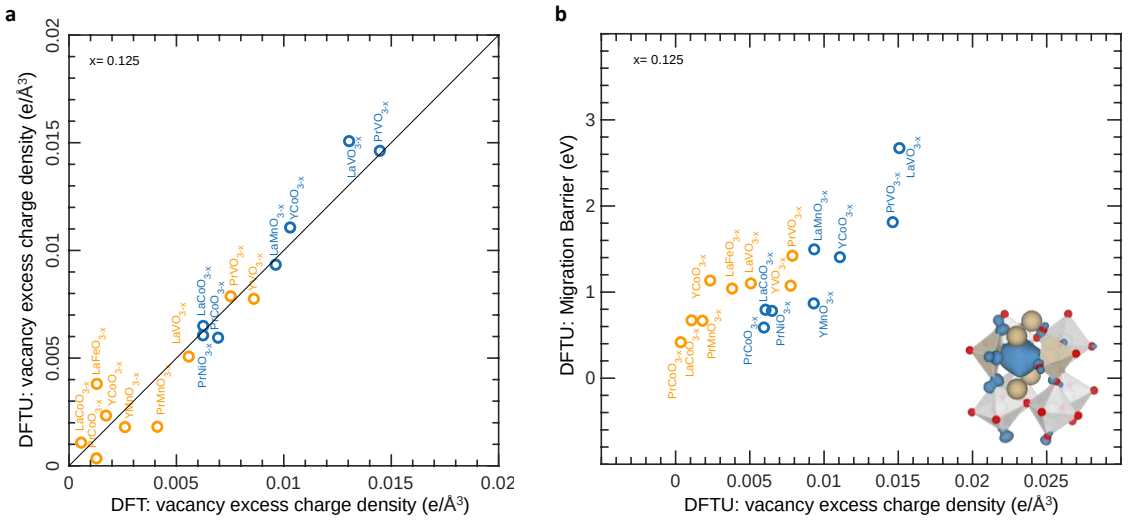

Figure S18. Correlation between migration barrier and vacancy excess charge density with PBE+U formalism. a) Comparison between vacancy excess charge density with PBE+U and PBE formalism. b) Comparison between migration barrier and vacancy excess charge density with PBE+U formalism (Pearson correlation coefficient=0.82). Data are tabulated in Table S4.

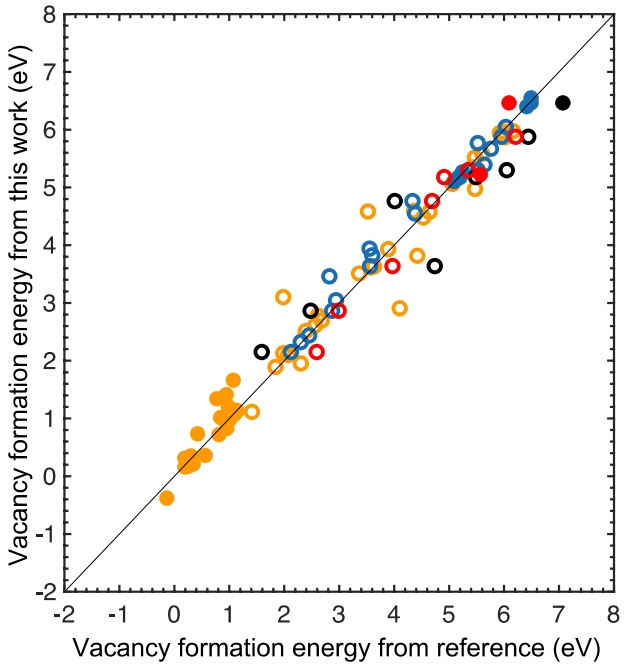

Figure S19. Comparison between vacancy formation energies in this work and computational literature. Empty and solid circles correspond to oxides with and without d electrons, respectively. Orange datapoints correspond to CC vacancy formation energies from this work compared to those reported in Ref.[16]. Blue datapoints correspond to NCC vacancy formation energies from this work compared to those reported in Ref.[16]. Black datapoints correspond to NCC migration barriers compared to those reported in Ref.[17], and grey datapoints correspond to CC migration barriers compared to those reported in Ref.[18]. The vacancy formation energies from Mayeshiba and Morgan[16] were reported at 1073 K and 1 bar and we referenced at 0K for comparison with our data. Data extracted from the literature are tabulated in Table S7.

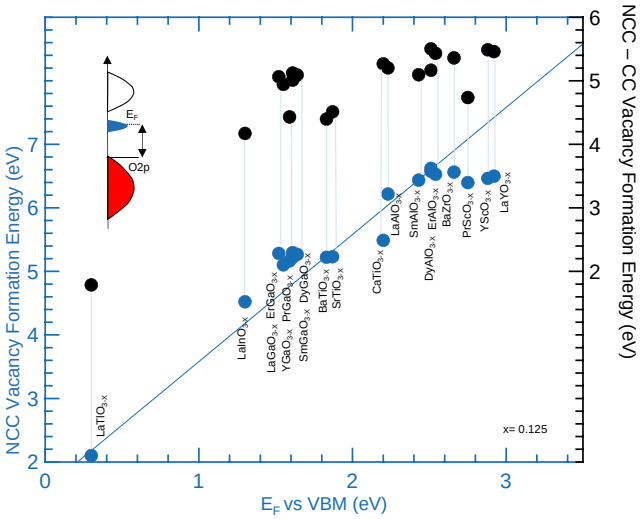

Figure S20. Electronic origin of increased NCC vacancy formation energy penalty in oxides without d electrons. Comparison between the NCC vacancy formation energy and the energy highest occupied states referenced to the valence band maximum (VBM), as shown in the schematic. Comparison between the increased NCC vacancy formation energy vs. the CC vacancy formation energy (right vertical axis) and energy highest occupied states referenced to the valence band maximum (VBM) is also shown by the black datapoint. The blue continuous line (y=2x) is shown.

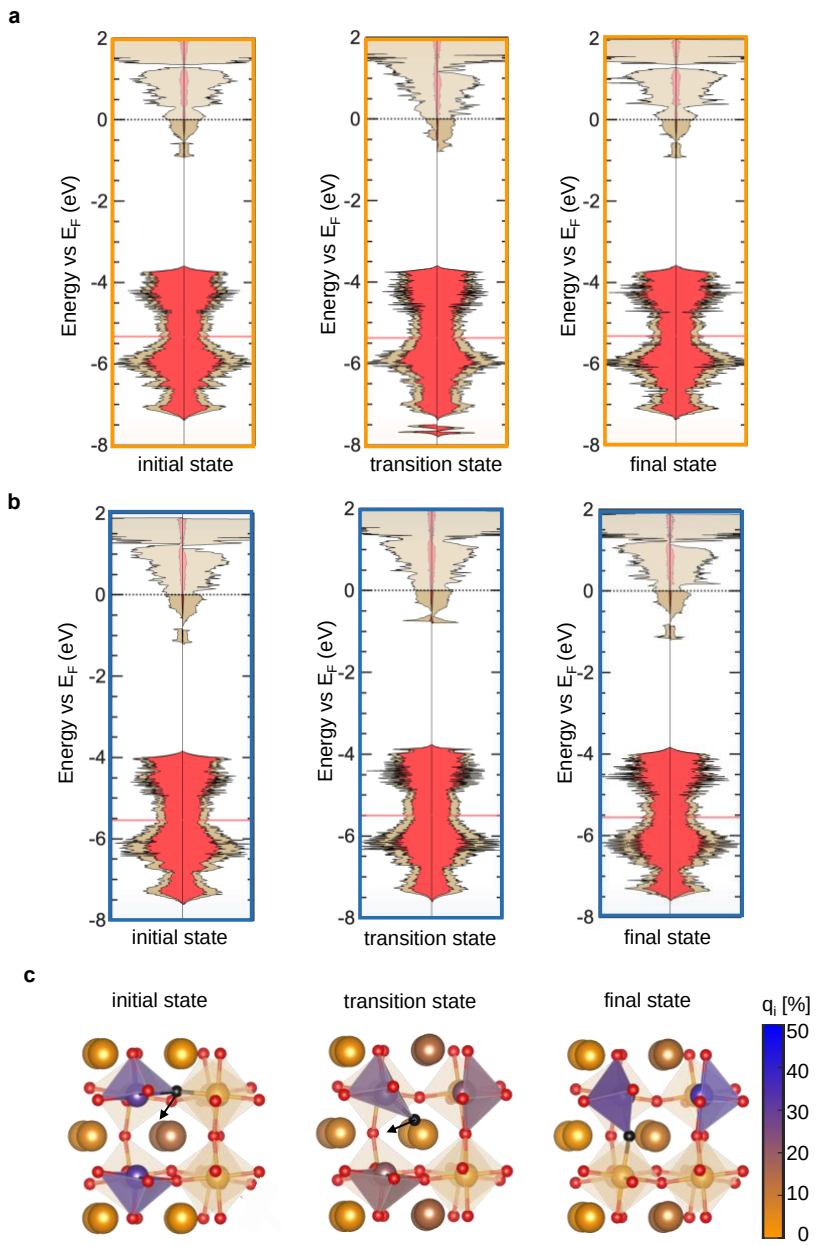

Figure S21. Signatures of ion migration in the DOS of $LaTiO_{2.875}$. (a) Computed DOS for $LaTiO_{2.875}$ with (a) CC and (b) NCC oxygen vacancies for initial (left), transition (center), and final state (right) during oxygen ion migration. (c) Visualization of normalized atomic excess charge in NCC $LaTiO_{2.875}$ during migration. Colors indicate the normalized atomic excess charge density from orange (0%) to blue (50%). The migration oxygen ion is in black and its direction is highlighted by the black arrow. The atomic excess charge is evaluated as described in the supplementary computational methods.

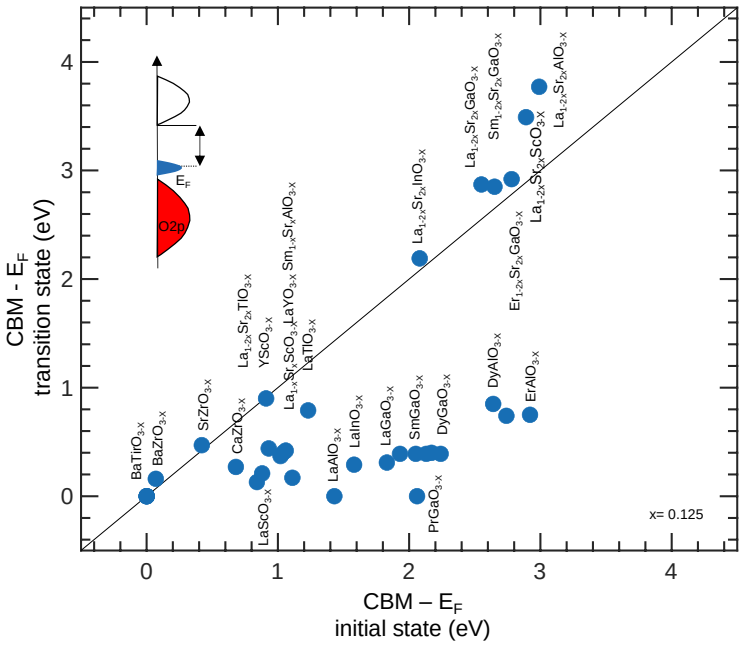

Figure S22. Changes in the energy of conduction band minimum vs. filled localized states from equilibrium to transition state. A schematic is shown at the top left to depict how the axes were computed.

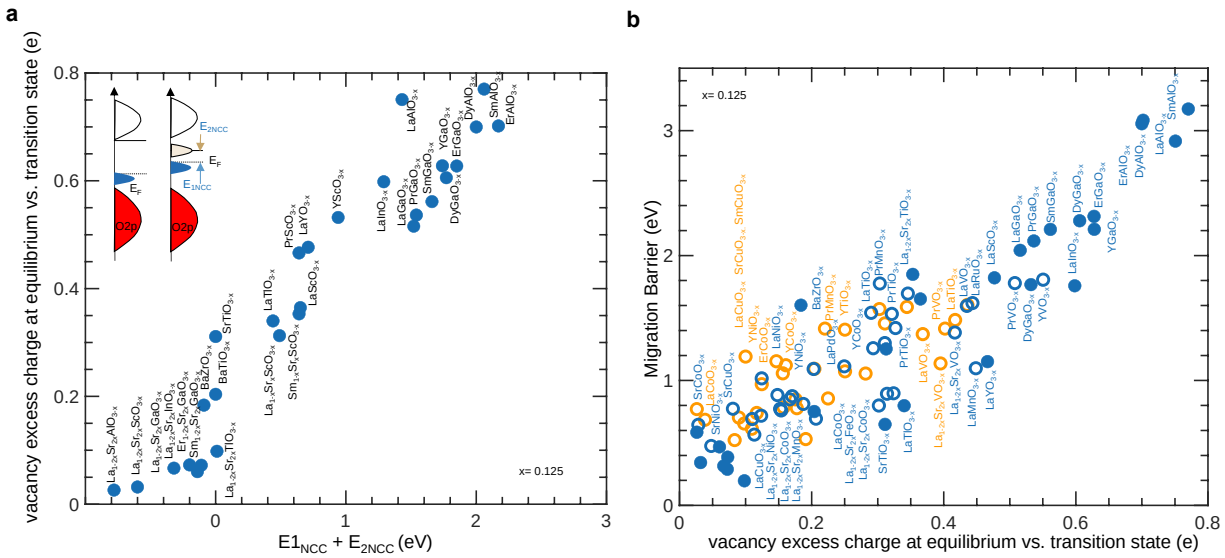

Figure S23. Trends in filled vacancy states, charge screening, and migration barrier in the transition state. (a) Comparison between the charge screening from equilibrium to saddle point (computed as the difference between vacancy excess charge between initial and transition state) and E_{1NCC}+E_{2NCC} (highlighted by the top right schematic and in Figure 6a). (b) Comparison between the migration barrier and charge screening from equilibrium to saddle point. The vacancy excess charge is evaluated as described in the supplementary computational methods.

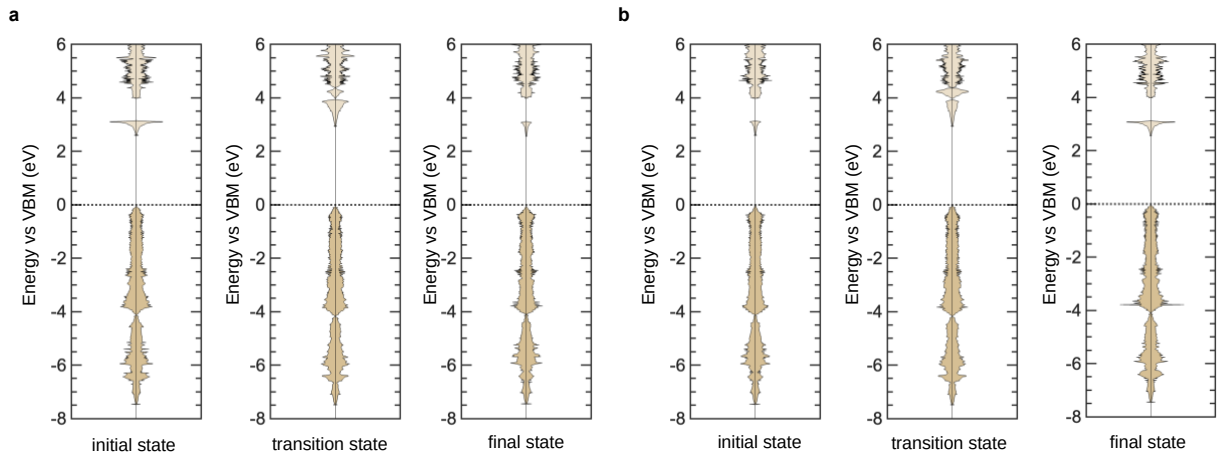

Figure S24. **Site projected DOS of Ga atoms in CC $LaGaO_{2.875}$ during migration.** Computed DOS projected on the Ga atom (a) forming a bond and (b) breaking a bond with the migrating oxygen ion for the initial (left), transition (center), final (right) state.

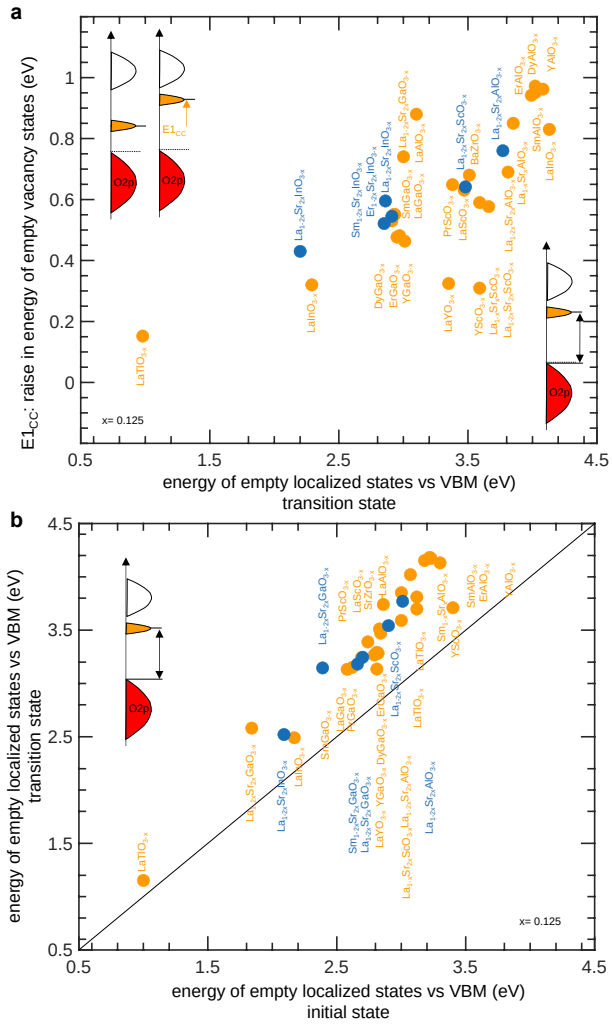

Figure S25. Changes in the energy of empty localized states associated with oxygen vacancies. (a) Comparison between the variation in energy of empty localized states during oxygen migration (E_{1CC} as highlighted in the schematic and in Figure 7a) and the energy of empty localized states vs. VMB at transition state. (b) Comparison between the energy of empty localized states at transition vs. initial state (horizontal axis). A schematic is shown at the top left to depict how the axes were computed.

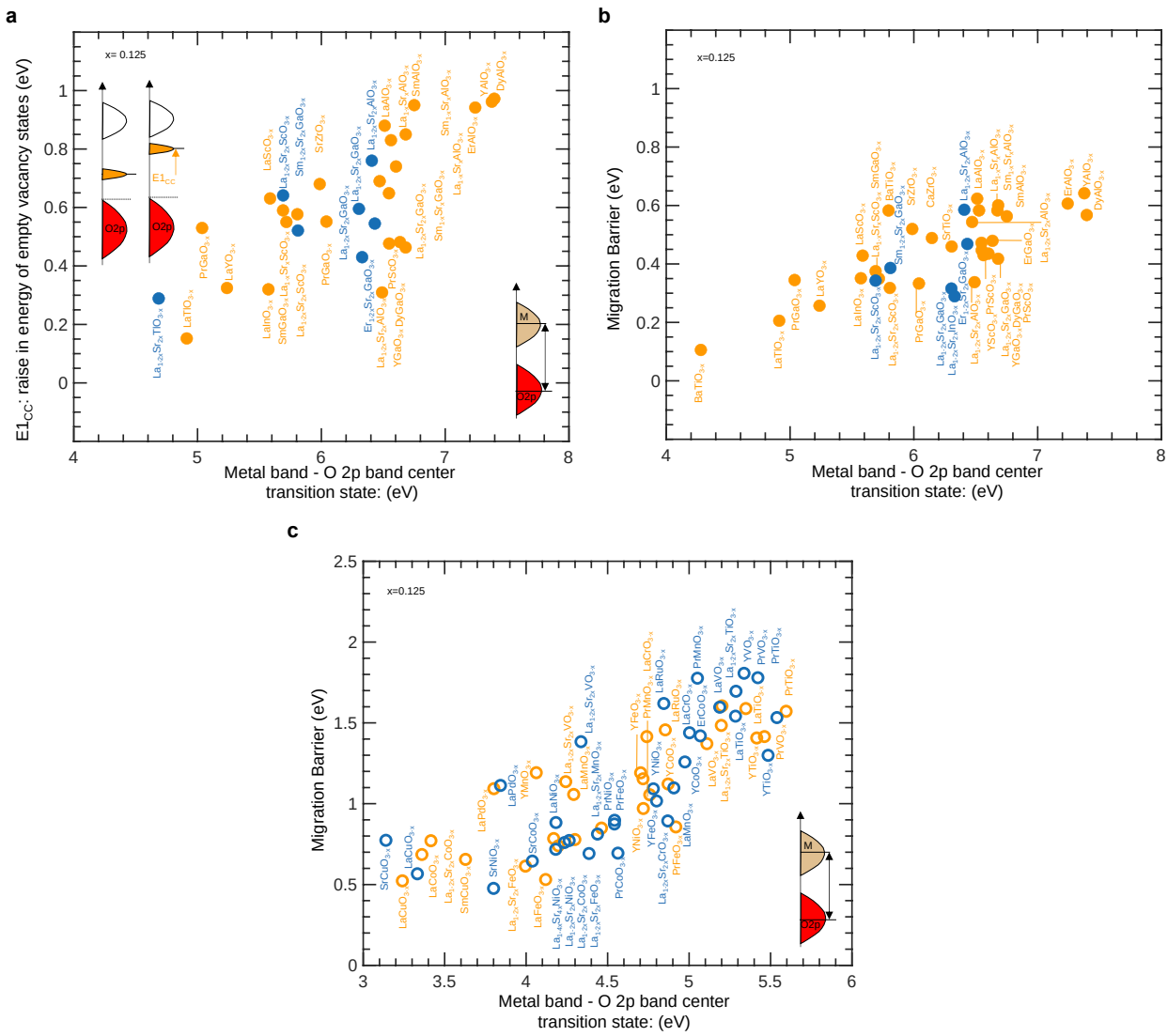

Figure S26. Trends of empty vacancy states, covalency, and migration barriers at the transition state. (a) Comparison between E_{1CC} (as highlighted in the schematic and in Figure 7a) and the energy of metal states vs. the O 2p band center at the transition state. Comparison between migration barrier and the energy of metal states vs. the O 2p band center at the transition state for perovskites (b) without and. (c) with d electrons.

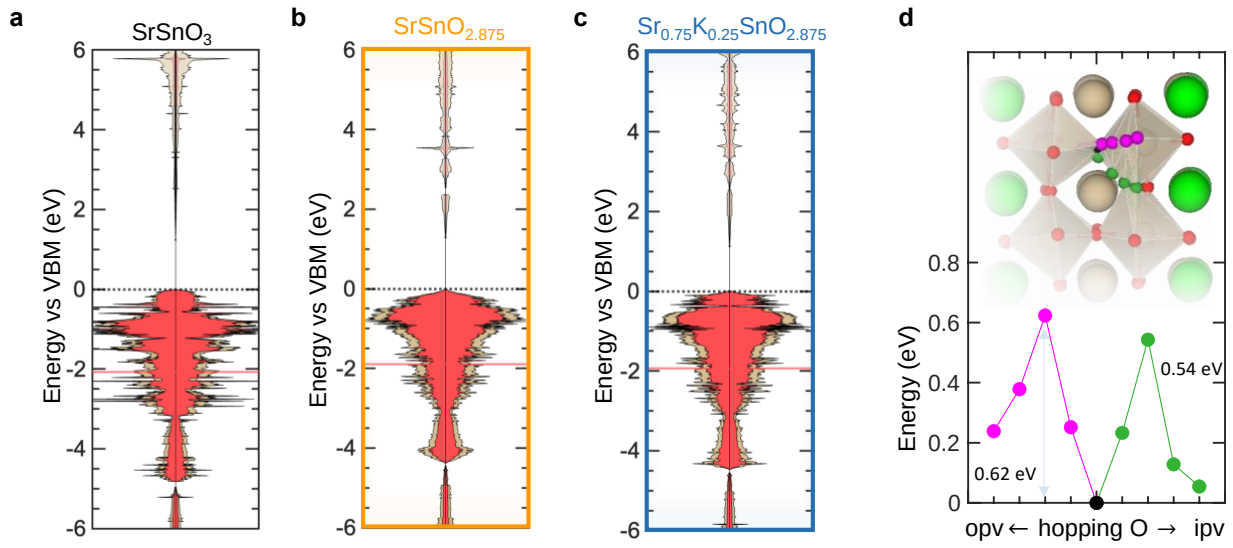

Figure S27. Oxygen ion transport in $Sr_{0.75}K_{0.25}SnO_{2.875}$**.** (a) Computed electronic structure of $SrSnO_3$, (b) CC $SrSnO_{2.875}$, (c) NCC $Sr_{0.75}K_{0.25}SnO_{2.875}$. (d) Energy landscape of two different migration pathways, as shown in the top schematic. Substituent K atoms are highlighted in green, the hopping ion is in black and the two opv and ipv migration pathways are highlighted in green and magenta, respectively.

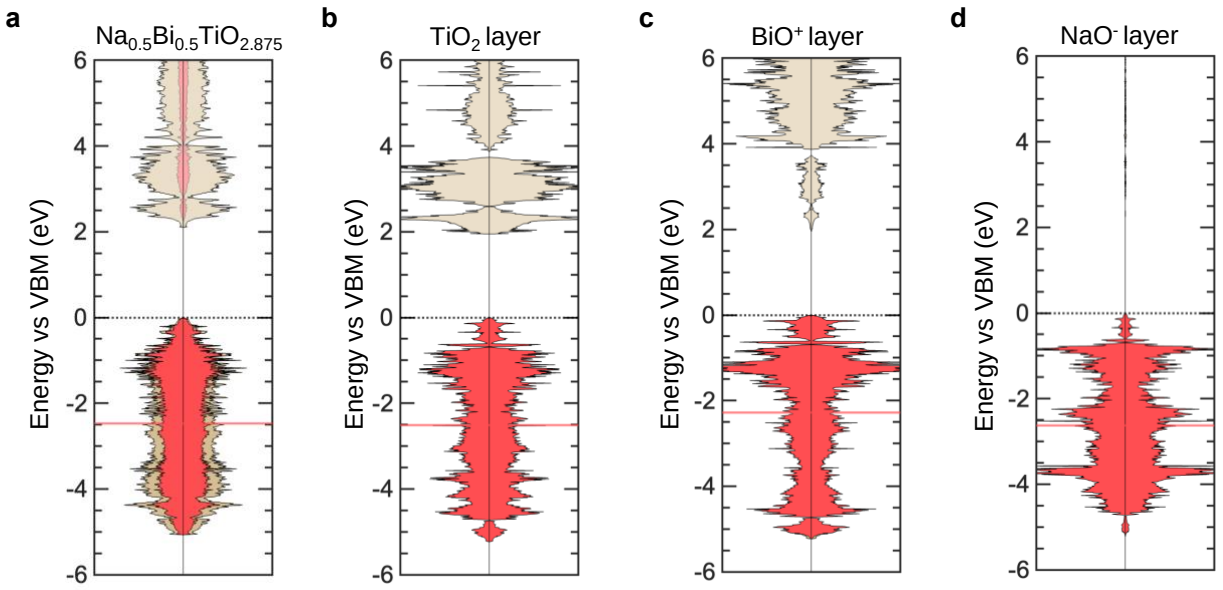

Figure S28. Electronic structure of $Na_{0.5}Bi_{0.5}TiO_{2.875}$. Computed electronic DOS of (a) $Na_{0.5}Bi_{0.5}TiO_{2.875}$ and projections onto atoms belonging to the (b) TiO_2, (c) BiO^+ and (d) NaO^- layers. The O 2p band center is highlighted by the red horizontal line.

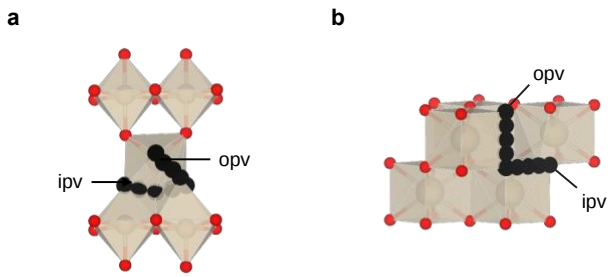

Figure S29. Computed migration pathways. (a) In the rutile crystal structure, the opv pathway was computed from an apical to an equatorial site along the edge of one MO_6 octahedron, and the ipv pathway was computed from one apical site to the next apical site along the a-axis. (b) In the fluorite crystal structure, the opv and ipv migration pathways were computed along two edges of the MO_8 cube.

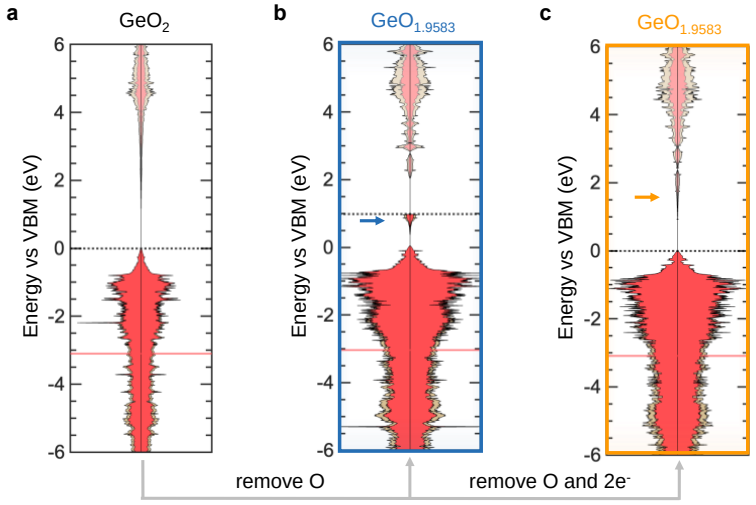

Figure S30. Electronic signatures of oxygen vacancies in rutile GeO_{2-x}. Computed electronic DOS of (a) GeO_2, $GeO_{1.9583}$ with (b) NCC and (c) CC oxygen vacancies.

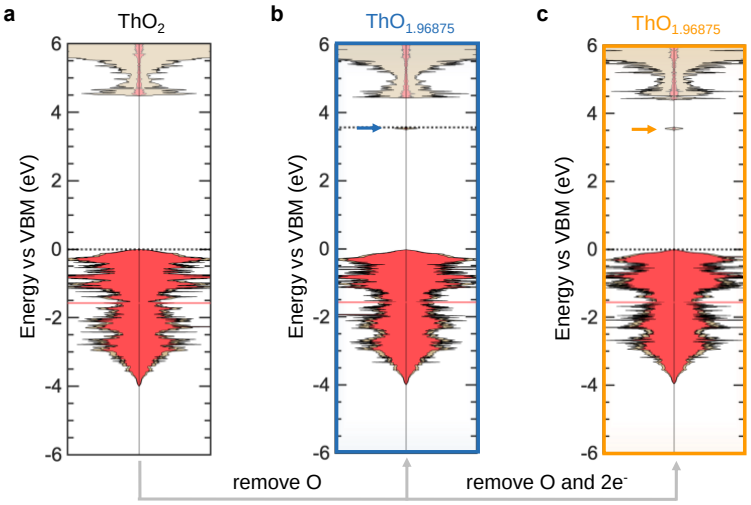

Figure S31. Electronic signatures of oxygen vacancies in rutile HfO_{2-x}. Computed electronic DOS of (a) HfO_2, $HfO_{1.96875}$ with (b) NCC and (c) CC oxygen vacancies.

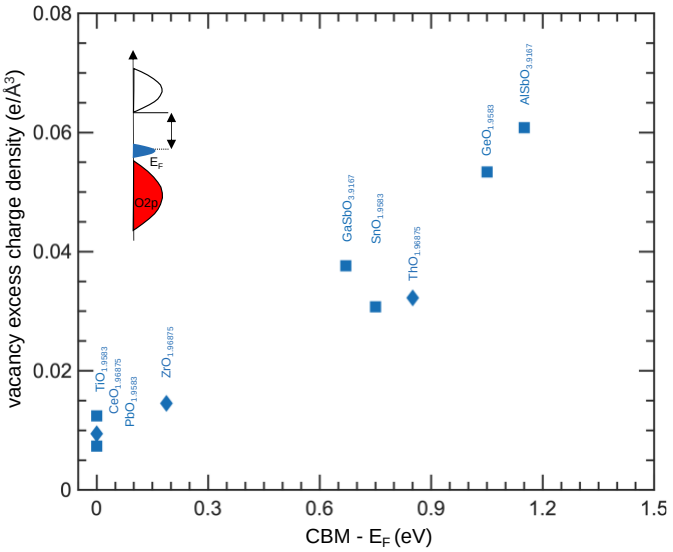

Figure S32. Correlation between vacancy excess charge density and energy of vacancy states relative to CBM for rutile and fluorite structures. The vacancy excess charge density was computed considering three and four neighboring cations to the oxygen vacancy for rutile (squares) and fluorite (diamonds) structures, respectively. A schematic is shown at the top left to depict how the energy of vacancy states relative to CBM was computed.

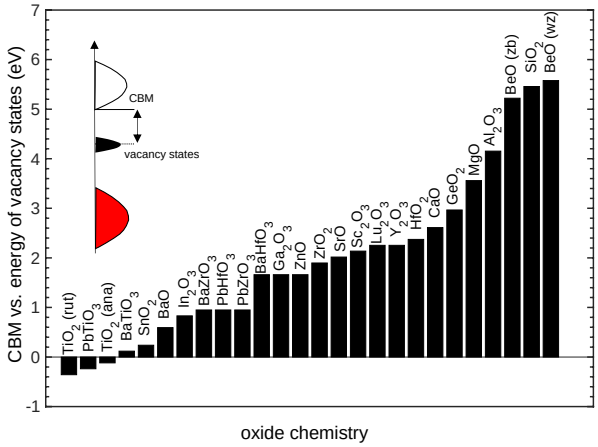

Figure S33. Trends of migration barrier with the energy of vacancy states. (a) Sorted values of energy of vacancy states relative to the conduction band minimum (CBM) extracted from reference.[19]

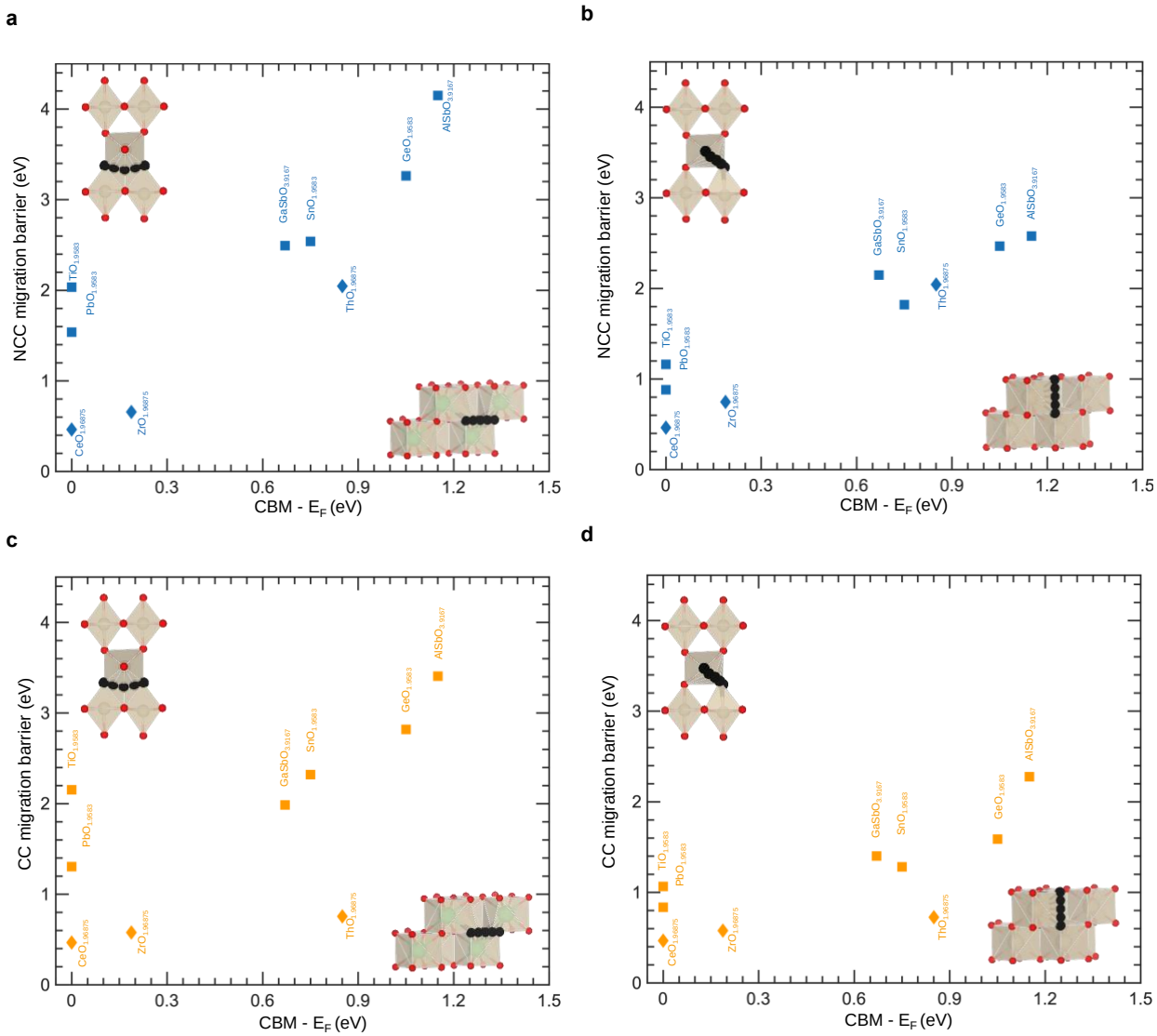

Figure S34. Comparison between migration barrier and energy of vacancy states relative to CBM for rutile and fluorite structures. (a) ipv and (b) opv NCC migration barriers, (c) ipv and (d) opv CC migration barriers. A schematic of the pathway is included for rutile (top left) and fluorite (bottom left) structures. Rutile and fluorite structures are labeled as squares and diamonds, respectively.

Supplementary Tables

Table S1. Crystal structure information and magnetic

moments for the obtaiend perfect perovskite structures. Magnetic moments of LaBO3 perovskites decrease with B changing in the order Fe > Cr > Co > V > Ni > Ti, consistent with experimentally reported values of 4.6+-0.2 for LaFeO3,[21] 2.8 +- 0.2 for LaCrO3,[21] 2 for LaCoO3 at 90K,[22] 1.4 for LaVO3,[23] 1 for LaNiO3,[24] and 0.45 for LaTiO3 at 10K.[25]

stoichiometric formula	lattice yype	spacegroup	lattice constants (Å)			lattice angles (°)			magnetic moment (μB/atom)
			a	b	c	α	β	γ	
BaInO3	orthorhombic	Pnma	8.549	8.527	8.549	90	89.19	90	0.2
BaTiO3	monoclinic	Pc	8.062	8.062	8.062	90	90	90	0.0
BaZrO3	orthorhombic	Imma	8.501	8.5	8.501	90	89.96	90	0.0
CaTiO3	monoclinic	Pc	7.879	7.874	7.879	90	89.91	90	0.0
CaZrO3	orthorhombic	Pnma	8.067	8.058	8.066	90	91.93	90	0.0
DyAlO3	orthorhombic	Pnma	7.487	7.436	7.487	90	91.77	90	0.0
DyGaO3	orthorhombic	Pnma	7.704	7.625	7.703	90	93.14	90	0.0
Er0.75Sr0.25GaO3	monoclinic	Pm	7.747	7.685	7.699	90	92.67	90	0.0
ErAlO3	orthorhombic	Pnma	7.458	7.398	7.458	90	92.23	90	0.0
ErCoO3	orthorhombic	Pnma	7.509	7.347	7.509	90	94.33	90	0.0
ErGaO3	orthorhombic	Pnma	7.663	7.6	7.662	90	93.32	90	0.0
La0.5Sr0.5NiO3	monoclinic	P2_1/m	7.805	7.621	7.645	90	89.29	90	0.1
La0.75Sr0.25AlO3	monoclinic	P2/m	7.876	7.871	7.863	90	89.54	90	0.0
La0.75Sr0.25CoO3	monoclinic	Pm	7.692	7.686	7.698	90.02	89.5	89.98	0.4
La0.75Sr0.25CrO3	monoclinic	Pm	7.801	7.795	7.798	90	89.92	90	0.6
La0.75Sr0.25FeO3	monoclinic	Pm	7.753	7.739	7.748	90.05	89.67	90.04	0.7
La0.75Sr0.25GaO3	monoclinic	Pm	7.876	7.871	7.863	90	89.54	90	0.0
La0.75Sr0.25InO3	monoclinic	Pm	8.345	8.346	8.332	90	92.11	90	0.1
La0.75Sr0.25MnO3	monoclinic	Pm	7.827	7.819	7.816	90	89.82	90	0.6
La0.75Sr0.25NiO3	monoclinic	Pm	7.708	7.701	7.696	90	89.43	90	0.1
La0.75Sr0.25ScO3	monoclinic	Pm	8.176	8.148	8.159	90	91.29	90	0.0
La0.75Sr0.25TiO3	monoclinic	Pm	7.92	7.924	7.918	90	90.37	90	0.1
La0.75Sr0.25TlO3	monoclinic	Pm	8.556	8.588	8.537	90	93.08	90	0.0
La0.75Sr0.25VO3	monoclinic	Pm	7.845	7.825	7.843	90	90.01	90	0.4
La0.875Sr0.125AlO3	orthorhombic	Amm2	7.64	7.615	7.673	90	89.76	90	0.0
La0.875Sr0.125ScO3	monoclinic	Pm	8.156	8.139	8.19	90	91.37	90	0.0
LaAlO3	orthorhombic	Imma	7.64	7.615	7.673	90	89.76	90	0.0
LaCoO3	orthorhombic	Pnma	7.724	7.725	7.759	90	89.76	90	0.3
LaCrO3	orthorhombic	Pnma	7.844	7.824	7.844	89.99	90.26	90.01	0.6
LaCuO3	orthorhombic	Pnma	7.81	7.789	7.81	90	89.7	90	0.0
LaFeO3	orthorhombic	Pnma	7.804	7.789	7.805	90	90.08	90	0.7
LaGaO3	orthorhombic	Pnma	7.874	7.87	7.875	90	90.27	90	0.0
LaInO3	orthorhombic	Pnma	8.325	8.334	8.325	90	92.31	90	0.0
LaMnO3	orthorhombic	Pnma	7.892	7.864	7.895	90	90.5	90.01	0.8
LaNiO3	orthorhombic	Pnma	7.715	7.726	7.715	90	89.76	90	0.1
LaPdO3	orthorhombic	Pnma	8.273	7.855	8.273	90	93.89	90	0.0
LaRuO3	orthorhombic	Pnma	8.06	7.911	8.059	90	94.76	90	0.2
LaScO3	orthorhombic	Pnma	8.156	8.139	8.19	90	91.37	90	0.0
LaTiO3	orthorhombic	Pnma	7.939	7.931	7.939	89.99	90.86	90.01	0.0
LaTlO3	orthorhombic	Pnma	8.516	8.604	8.553	90	93.22	90	0.0

LaVO3	orthorhombic	Pnma	7.873	7.877	7.873	90	90.43	90	0.2
LaYO3	orthorhombic	Pnma	8.507	8.589	8.507	90	92.04	90	0.0
PrCoO3	orthorhombic	Pnma	7.718	7.693	7.751	89.94	90.44	90.14	0.3
PrFeO3	orthorhombic	Pnma	7.81	7.731	7.769	90	90.87	89.99	0.7
PrGaO3	orthorhombic	Pnma	7.849	7.828	7.849	90	90.88	90	0.0
PrMnO3	orthorhombic	Pnma	7.876	7.824	7.876	90	91.18	90	0.8
PrNiO3	orthorhombic	Pnma	7.691	7.69	7.69	90	90.09	90	0.1
PrScO3	orthorhombic	Pnma	8.123	8.102	8.123	90	92.05	90	0.0
PrTiO3	orthorhombic	Pnma	7.931	7.879	7.932	90	91.67	90	0.2
PrVO3	orthorhombic	Pnma	7.862	7.84	7.895	90	91.41	90	0.2
Sm0.75Sr0.25GaO3	monoclinic	Pm	7.831	7.777	7.803	90	91.47	90	0.1
Sm0.875Sr0.125AlO3	monoclinic	Pm	7.546	7.537	7.546	90	90.39	90	0.0
SmAlO3	orthorhombic	Pnma	7.546	7.537	7.546	90	90.39	90	0.0
SmCuO3	orthorhombic	Pnma	7.76	7.611	7.76	90	92.85	90	0.0
SmGaO3	orthorhombic	Pnma	7.794	7.726	7.794	90	92.21	90	0.0
SrCoO3	orthorhombic	Imma	7.673	7.667	7.672	90	89.91	90	0.5
SrCuO3	orthorhombic	Imma	7.757	7.778	7.757	90	89.76	90	0.1
SrNiO3	orthorhombic	Pmc2_1	7.674	7.743	7.672	90	89.56	90	0.0
SrTiO3	orthorhombic	Imma	7.879	7.874	7.879	90	89.91	90	0.0
SrZrO3	orthorhombic	Pnma	8.273	8.259	8.273	90	90.5	90	0.0
YAlO3	orthorhombic	Pnma	7.489	7.432	7.489	90	91.87	90	0.0
YCoO3	orthorhombic	Pnma	7.556	7.412	7.556	90.01	93.74	89.99	0.0
YCrO3	orthorhombic	Pnma	7.687	7.598	7.691	90.01	93.37	89.99	0.6
YFeO3	orthorhombic	Pnma	7.707	7.533	7.708	90	94.1	90.01	0.7
YGaO3	orthorhombic	Pnma	7.72	7.636	7.719	90	93.03	90	0.0
YMnO3	orthorhombic	Pnma	7.769	7.602	7.768	90.01	93.83	90.01	0.8
YNiO3	orthorhombic	Pnma	7.632	7.413	7.631	89.99	93.89	90.01	0.2
YScO3	orthorhombic	Pnma	7.929	7.981	7.929	90	92.97	90	0.0
YTiO3	orthorhombic	Pnma	7.817	7.695	7.85	90	93.79	90.01	0.2
YVO3	orthorhombic	Pnma	7.728	7.637	7.728	89.99	93.8	90	0.4

Table S2. Computed NCC and CC vacancy formation energies and migration barriers.

chemical formula	CC Migration Barrier (eV)	NCC Migration Barrier (eV)	CC Vacancy Formation Energy (eV)	NCC Vacancy Formation Energy (eV)
BaInO2.875	0.5832	0.5809	-0.7053	-0.5488
BaTiO2.875	0.5830	0.7515	0.7194	5.2307
BaZrO2.875	0.5831	1.6027	1.2024	6.5627
CaTiO2.875	0.1058	0.3105	0.2214	5.4882
CaZrO2.875	0.4888		0.8399	
DyAlO2.875	0.5675	3.0553	1.4105	6.5755
DyGaO2.875	0.4470	2.2789	0.1735	5.2951
Er0.75Sr0.25GaO2.875		0.4685		0.1990
ErAlO2.875	0.6066	3.0829	1.1190	6.6217
ErCoO2.875	1.1541	1.4199	3.1014	3.5339
ErGaO2.875	0.4791	2.3137	0.2190	5.2830
La0.5Sr0.5NiO2.875		0.7182		0.8399
La0.75Sr0.25AlO2.875	0.5435	0.5854	0.2831	0.4973
La0.75Sr0.25CoO2.875	0.7709	0.7599	1.9526	2.2952
La0.75Sr0.25CrO2.875	1.2327	0.8934	3.8170	4.4030
La0.75Sr0.25FeO2.875	0.6138	0.6919	3.5103	3.2440
La0.75Sr0.25GaO2.875	0.4354	0.3158	-0.3794	-0.1453
La0.75Sr0.25InO2.875		0.2894		0.0716
La0.75Sr0.25MnO2.875	0.7783	0.8122	2.9085	3.1570
La0.75Sr0.25NiO2.875	0.7398	0.7724	1.1135	1.3973
La0.75Sr0.25ScO2.875	0.3180	0.3430	0.3598	0.5487
La0.75Sr0.25TiO2.875	1.6051	1.6958	5.9760	5.9676
La0.75Sr0.25TlO2.875		0.1969		-0.1954
La0.75Sr0.25VO2.875	1.1365	1.3838	4.9747	5.1445
La0.875Sr0.125AlO2.875	0.6007	1.7981	0.5521	3.3154
La0.875Sr0.125ScO2.875	0.3755	1.2530	0.6204	2.3546
LaAlO2.875	0.6235	2.9162	1.0157	6.2177
LaCoO2.875	0.6857	0.7995	2.6089	2.8650
LaCrO2.875	1.0554	1.4389	#DIV/0!	5.1785
LaCuO2.875	0.5227	0.5666	0.8457	1.1526
LaFeO2.875	0.5310	0.8489	3.6144	3.6392
LaGaO2.875	0.3332	2.0420	0.1601	5.1021
LaInO2.875	0.3510	1.7581	0.3516	4.5221
LaMnO2.875	1.0573	1.0980	4.5934	4.7650
LaNiO2.875	0.7845	0.8834	1.8937	2.1513
LaPdO2.875	1.0930	1.1132	2.1276	2.1134
LaRuO2.875	1.4567	1.6200	3.9316	4.0001
LaScO2.875	0.4285	1.8220	0.9759	6.4640
LaTiO2.875	1.4843	1.5418	5.9663	5.8765
LaTlO2.875	0.2056	0.7982	0.3135	2.1002
LaVO2.875	1.3713	1.5972	5.3475	5.2981
LaYO2.875	0.2572	1.1511	1.0400	6.4989
PrCoO2.875	0.7020	0.6942	2.7809	3.0466
PrFeO2.875	0.8563	0.8976	3.6301	3.8243
PrGaO2.875	0.3450	2.1174	0.7346	5.1656

PrMnO2.875	1.4152	1.7766	4.4810	4.5458
PrNiO2.875	0.8492	0.8745	2.0993	2.3237
PrScO2.875	0.4724	1.8495	1.6620	6.3980
PrTiO2.875	1.5719	1.5329	5.8665	5.6700
PrVO2.875	1.4154	1.7797	5.5188	5.7685
Sm0.75Sr0.25GaO2.875		0.3862		-0.1773
Sm0.875Sr0.125AlO2.875	0.4302	1.6524	0.3936	3.3353
SmAlO2.875	0.5631	3.1735	1.3416	6.4367
SmCuO2.875	0.6557		1.1326	
SmGaO2.875	0.3499	2.2095	0.2108	5.2202
SrCoO2.875		0.6450		0.6536
SrCuO2.875	0.7032	0.7737	-0.9861	-0.7251
SrNiO2.875		0.4760		-0.2452
SrTiO2.875	0.4597	0.6485	0.8256	5.2225
SrZrO2.875	0.5197	1.4870	1.2203	6.6308
YAlO2.875	0.6419		1.0963	6.5283
YCoO2.875	1.1221	1.2584	2.6950	3.4609
YCrO2.875	1.0730		5.0608	
YFeO2.875	1.1914	1.0170	4.5835	3.9407
YGaO2.875	0.4177	2.2103	0.1776	5.2677
YMnO2.875	1.1922		4.5742	
YNiO2.875	0.9704	1.0922	2.5122	2.4385
YScO2.875	0.3378	1.7675	1.0802	6.5493
YTiO2.875	1.4067	1.2995	5.9420	6.0474
YVO2.875	1.5887	1.8070	5.5840	5.3934

Table S3. Computed electronic descriptors of migration barrier and vacancy formation energy. The orbital overlap was computed as the relative position of filled metal d and O 2p bands for oxides with d electrons while for oxides without d electrons and localized charge it was computed as the relative position of the lowest unoccupied metal states vs. the top filled localized states (as defined by the Fermi level).

chemical formula	O 2p Band Center vs E_F (eV) Figure 1c	CC O 2p Band Center vs E_F (eV) Figure 5b	NCC O 2p Band Center vs E_F (eV) Figure 5b	NCC Orbital overlap (eV) Figure 1d	CC Orbital overlap (eV) Figure 1d	CC vacancy excess charge density (e/Å^3) Figure 1e	NCC vacancy excess charge density (e/Å^3) Figure 1e
BaInO2.875	-1.450	-1.430	-1.464			0.000	0.002
BaTiO2.875	-1.896	-2.023	-4.158	0.000		0.000	0.006
BaZrO2.875	-1.608	-1.732	-4.935	0.070		0.000	0.011
CaTiO2.875	-1.732	-1.989	-4.543	0.000		0.000	0.006
CaZrO2.875	-1.456	-1.543		0.680		0.001	
DyAlO2.875	-2.089	-2.129	-4.807	2.731		0.000	0.023
DyGaO2.875	-1.803	-1.855	-3.696	2.161		0.001	0.019
Er0.75Sr0.25GaO2.875	-1.815		-1.912				0.003
ErAlO2.875	-2.113	-2.104	-4.821	2.911		0.000	0.025
ErCoO2.875	-3.776	-3.728	-4.060	1.996	1.717	0.002	0.012
ErGaO2.875	-1.839	-1.849	-3.665	2.231		0.001	0.020
La0.5Sr0.5NiO2.875	-2.663		-2.837	0.719			-0.019
La0.75Sr0.25AlO2.875	-1.907	-1.934	-5.066			0.000	0.002
La0.75Sr0.25CoO2.875	-3.413	-3.421	-3.593	1.086	0.740	0.000	0.005
La0.75Sr0.25CrO2.875	-3.817	-3.929	-4.005	1.546	1.345	0.001	0.009
La0.75Sr0.25FeO2.875	-4.014	-3.857	-4.165	0.912	0.495	0.000	0.007
La0.75Sr0.25GaO2.875	-1.778	-1.815	-1.917			0.000	0.003
La0.75Sr0.25InO2.875	-1.421		-1.518				0.003
La0.75Sr0.25MnO2.875	-3.030	-3.858	-4.227	1.037	0.837	0.004	0.006
La0.75Sr0.25NiO2.875	-2.901	-2.827	-3.103	1.003	0.734	0.001	0.005
La0.75Sr0.25ScO2.875	-1.397	-1.429	-5.066	0.000		0.000	0.002
La0.75Sr0.25TiO2.875	-5.358	-5.087	-5.392	1.159	1.132	0.007	0.013
La0.75Sr0.25TlO2.875	-1.477		-1.518				0.003
La0.75Sr0.25VO2.875	-4.743	-4.805	-4.857	1.837	1.531	0.006	0.012
La0.875Sr0.125AlO2.875	-2.089	-2.170	-4.491	0.880		0.005	0.009
La0.875Sr0.125ScO2.875	-1.377	-1.424	-3.906	0.930		0.000	0.007
LaAlO2.875	-2.187	-2.262	-4.655	1.430		0.000	0.017
LaCoO2.875	-3.536	-3.843	-3.684	1.437	1.017	0.001	0.006
LaCrO2.875	-4.071	-3.495	-4.667	1.746	1.510	0.004	0.012
LaCuO2.875	-2.738	-2.655	-2.885	0.060	-0.193	0.000	0.004
LaFeO2.875	-4.227	-4.081	-4.311	1.128	0.816	0.001	0.008
LaGaO2.875	-1.815	-1.906	-3.641	1.831		0.000	0.015
LaInO2.875	-1.484	-1.522	-3.024	1.580		0.001	0.013
LaMnO2.875	-4.377	-4.022	-4.365	1.101	0.928	0.002	0.010
LaNiO2.875	-3.187	-3.121	-3.427	1.395	1.015	0.001	0.006
LaPdO2.875	-3.337	-3.169	-3.392	0.339	0.149	0.004	0.008
LaRuO2.875	-4.252	-4.165	-4.281	1.786	1.557	0.005	0.011

LaScO2.875	-1.449	-1.480	-4.564	0.840		0.000	0.013
LaTiO2.875	-5.589	-5.314	-5.538	1.547	1.107	0.008	0.014
LaTlO2.875	-1.794	-1.813	-2.055	1.230	1.230	0.000	0.009
LaVO2.875	-4.815	-4.780	-4.907	2.139	1.846	0.006	0.013
LaYO2.875	-1.214	-1.283	-5.405	1.040		0.000	0.012
PrCoO2.875	-3.566	-3.550	-3.766	1.654	1.215	0.001	0.007
PrFeO2.875	-4.282	-4.050	-4.335	1.159	0.774	0.003	0.008
PrGaO2.875	-1.797	-1.893	-3.673	1.931	0.000	0.001	0.016
PrMnO2.875	-4.406	-4.148	-4.537	1.196	1.017	0.004	0.011
PrNiO2.875	-3.287	-3.196	-3.492	1.364	1.063	0.002	0.006
PrScO2.875	-1.471	-1.513	-5.562	1.060		0.000	0.014
PrTiO2.875	-5.665	-5.391	-5.572	1.622	1.197	0.009	0.017
PrVO2.875	-4.958	-4.684	-4.898	2.165	1.810	0.008	0.014
Sm0.75Sr0.25GaO2.875	-1.754		-1.901	0.000			0.003
Sm0.875Sr0.125AlO2.875	-2.067	-2.152	-4.617	1.020		0.001	0.011
SmAlO2.875	-2.097	-2.243	-4.900	2.061		0.000	0.020
SmCuO2.875	-2.816	-2.735			-0.125	0.002	
SmGaO2.875	-1.771	-1.869	-3.669	2.041		0.001	0.017
SrCoO2.875	-2.865		-3.054	0.011			0.004
SrCuO2.875	-2.143	-2.152	-2.205	-0.737	-0.751	0.001	0.003
SrNiO2.875	-2.413		-2.482	0.255			0.002
SrTiO2.875	-2.129	-2.290	-4.492	0.000		0.000	0.008
SrZrO2.875	-1.517	-1.688	-4.883	0.420		0.001	0.013
YAlO2.875	-2.069	-2.103	-4.779	2.641		-0.001	0.022
YCoO2.875	-3.732	-3.668	-3.988	1.975	1.679	0.002	0.010
YCrO2.875	-4.131	-3.999			1.646	0.004	
YFeO2.875	-4.180	-3.914	-4.272	0.950	0.852	0.003	0.009
YGaO2.875	-1.773	-1.818	-3.673	2.121	2.121	0.001	0.019
YMnO2.875	-4.413	-4.182			0.928	0.003	
YNiO2.875	-3.460	-3.318	-3.559	1.268	1.038	0.003	0.008
YScO2.875	-1.594	-1.540	-5.721	1.110	1.110	0.000	0.017
YTiO2.875	-5.474	-5.381	-5.505	1.733	1.505	0.011	0.018
YVO2.875	-4.909	-4.779	-4.987	2.258	1.955	0.009	0.017

Table S4. DFT+U computed vacancy formation energies and migration barriers for selected oxides. The U correction values utilized were sourced in the Materials Project and are calibrated based on formation enthalpies of transition metal oxides.[26]

Compound	TM	U value	CC migration barrier (eV)	NCC migration barrier (eV)	CC vacancy formation energy (eV)	NCC vacancy formation energy (eV)	CC vacancy excess charge density (e/Å^3)	NCC vacancy excess charge density (e/Å^3)
LaCoO2.875	Co	3.32	0.6715	0.7945	2.7554	2.9754	0.0011	0.0061
LaFeO2.875	Fe	5.3	1.0409		4.6122		0.0038	
LaMnO2.875	Mn	3.9		1.4959		5.0961		0.0093
LaVO2.875	V	3.25	1.1008	2.6720	5.2753	5.6025	0.0051	0.0151
PrCoO2.875	Co	3.32	0.4176	0.5880	2.9285	3.2020	0.0003	0.0059
PrMnO2.875	Mn	3.9	0.6664		5.1267		0.0018	
PrNiO2.875	Ni	6.2		0.7813		2.3349		0.0065
PrVO2.875	V	3.25	1.4219	1.8120	5.4273	5.4799	0.0079	0.0146
YCoO2.875	Co	3.32	1.1336	1.4051	2.7802	3.1997	0.0023	0.0111
YMnO2.875	Mn	3.9		0.8683	4.6737	5.0874	0.0018	0.0093
YVO2.875	Y	3.25	1.0743		5.9157		0.0078	

Table S5. Kinetic electronic structure descriptors of migration barrier.

chemical formula	$E1_{CC}$ - Raise in energy of empty vacancy electronic states (eV) Figure 7b	$E1_{CC}$ - Raise in energy of empty vacancy electronic states (eV) Figure 7b	$E1_{NCC} + E2_{NCC}$ (eV) Figure 6c
BaTiO2.875			0
BaZrO2.875			-0.0901
CaTiO2.875			
DyAlO2.875		0.9721	1.9905
DyGaO2.875		0.4768	1.7605
Er0.75Sr0.25GaO2.875	0.545		
ErAlO2.875		0.9419	2.1606
ErGaO2.875		0.4816	1.8405
La0.75Sr0.25AlO2.875	0.7602	0.6901	
La0.75Sr0.25GaO2.875	0.5953	0.7403	
La0.75Sr0.25InO2.875	0.43		
La0.75Sr0.25ScO2.875	0.6415	0.5769	
La0.75Sr0.25TlO2.875	0.2888		
La0.875Sr0.125AlO2.875		0.8502	0.6701
La0.875Sr0.125ScO2.875		0.5901	0.4902
LaAlO2.875		0.88	1.4304
LaGaO2.875		0.5518	1.5204
LaInO2.875		0.32	1.2903
LaScO2.875		0.631	0.7102
LaTlO2.875		0.152	0.4401
LaYO2.875		0.3246	0.6401
PrGaO2.875		0.5299	1.5404
PrScO2.875		0.6488	0.6402
Sm0.75Sr0.25GaO2.875	0.5212		
Sm0.875Sr0.125AlO2.875		0.8302	0.6502
SmAlO2.875		0.9502	2.0605
SmGaO2.875		0.5503	1.6504
SrTiO2.875			0
SrZrO2.875		0.6802	-0.0501
YAlO2.875		0.9621	1.7904
YGaO2.875		0.4633	1.7304
YScO2.875		0.3094	0.9403

Table S6. Experimental data gathered from literature for comparison with computation.

chemical formula	experimental chemical formula	Experimental migration barrier (eV)	Reference
BaTiO2.875	BaTiO3-x	0.70	9
CaTiO2.875	CaTiO3-x	0.49	5
DyAlO2.875	Dy0.975Ca0.025AlO3-x	1.24	14
La0.75Sr0.25AlO2.875	La0.8Sr0.2AlO2.9	0.91	13
La0.75Sr0.25GaO2.875	La0.9Sr0.1GaO3-x	0.60	12
La0.75Sr0.25InO2.875	La0.9Sr0.1InO3	0.70	12
La0.75Sr0.25ScO2.875	$La_{0.9}Sr_{0.1}ScO_{3-x}$	0.47	8
La0.875Sr0.125AlO2.875	La0.9Sr0.1AlO3	0.95	8
LaAlO2.875	LaAlO3-x; cubic	0.65	11
LaGaO2.875	La0.9Sr0.1GaO3	0.60	12
LaInO2.875	La0.9Sr0.1InO3	0.70	12
LaScO2.875	$La_{0.9}Sr_{0.1}ScO_{3-x}$	0.47	8
PrGaO2.875	Pr0.93Ca0.07Ga0.85Mg0.15O3-x	0.65	15
SrTiO2.875	SrTiO3-x	0.65	9
La0.75Sr0.25CoO2.875	$La_{0.75}Sr_{0.25}CoO3$-x	0.82	5
La0.75Sr0.25CrO2.875	La0.9Ca0.12CrO3-x	1.74	7
La0.75Sr0.25FeO2.875	$La_{0.9}Sr_{0.1}FeO_{3-x}$	0.77	5
La0.75Sr0.25MnO2.875	La0.79Sr0.2MnO3	0.73	6
LaCoO2.875	LaCoO3	0.80	5
LaCrO2.875	La0.9Ca0.12CrO3-x	1.74	7
LaFeO2.875	$LaFeO_{3-x}$	0.77	5

Table S7. Computational data gathered from literature for comparison. MB refers to "migration barrier" and Evac refers to "vacancy formation energy". The vacancy formation energies in Ref.[16] are reported at 1073K and 1 bar and were referenced at 0K for comparison with the data from this work by adding a conversion factor for the energy of oxygen at 0K (+0.902 eV).

Chemical Formula	CC MB from Ref.[16] (eV)	CC MB from Ref.[14] (eV)	NCC MB from Ref.[16] (eV)	NCC MB from Ref.[17] (eV)	CC Evac from Ref.[16] (eV)	NCC Evac MB from Ref.[16] (eV)	NCC Evac MB from Ref.[17] (eV)	NCC Evac MB from Ref.[18] (eV)
BaTiO2.875	0.67				-0.09			
BaZrO2.875	0.69				0.08			
DyAlO2.875	0.55	0.38			0.04			
DyGaO2.875	0.44				-0.65			
ErAlO2.875	0.59				0.11			
ErCoO2.875	1.22				1.08			
ErGaO2.875	0.47				-0.62			
La0.75Sr0.25CoO2.875	0.79				1.40			
La0.75Sr0.25CrO2.875	1.17				3.52			
La0.75Sr0.25FeO2.875	1.00				2.46			
La0.75Sr0.25GaO2.875	0.39				-1.04			
La0.75Sr0.25MnO2.875	0.97				3.20			
La0.75Sr0.25NiO2.875	0.85				0.51			
La0.75Sr0.25ScO2.875	0.51				-0.34			
La0.75Sr0.25TiO2.875	1.55				5.26			
La0.75Sr0.25VO2.875	1.33				4.57			
LaAlO2.875	0.64	0.87			-0.06			
LaCoO2.875	0.70		0.76	0.76	1.66	1.97	2.48	2.99
LaCrO2.875	0.97		1.67	1.75	3.92	4.29	5.49	4.91
LaFeO2.875	0.83		0.81	0.85	2.67	2.66	4.74	3.97
LaGaO2.875	0.35		2.07		-0.71	4.19		
LaInO2.875	0.39				-0.60			
LaMnO2.875	0.75		0.94		3.46	3.43	4.01	4.69
LaNiO2.875	0.81		0.90	0.80	0.94	1.22	1.59	2.59
LaPdO2.875	1.04				1.08			
LaRuO2.875	1.43				2.99			
LaScO2.875	0.46		1.97	1.80	0.10	5.59	7.07	6.09
LaTiO2.875	1.60		1.61	1.65	5.09	5.05	6.44	6.21
LaTlO2.875	0.21				-0.71			
LaVO2.875	1.36		1.63	1.58	4.52	4.62	6.05	5.35
LaYO2.875	0.32				0.15			
PrCoO2.875	0.68		0.76		1.71	2.04		
PrFeO2.875	0.80		0.83		2.73	2.70		
PrGaO2.875	0.35		2.13		-0.48	4.26		
PrMnO2.875	0.75		1.03		3.63	3.48		
PrNiO2.875	0.85		0.88		1.17	1.40		
PrScO2.875	0.49		2.03		0.17	5.51		
PrTiO2.875	1.62		1.54		5.11	4.86		
PrVO2.875	1.46		1.75		4.57	4.62		
SmAlO2.875	0.55	0.53			-0.13			

SmCuO2.875	0.66		0.23		
SmGaO2.875	0.36		-0.56		
SrTiO2.875	0.46		0.05		5.57
YCoO2.875	1.17	1.47	1.78	1.92	
YCrO2.875	1.22	2.16	4.16	4.45	
YFeO2.875	1.29	0.97	2.62	2.65	
YGaO2.875	0.43	2.33	-0.68	4.34	
YMnO2.875	0.93	1.26	3.74	3.51	
YNiO2.875	1.11	1.22	1.49	1.55	
YScO2.875	0.42	1.90	0.20	5.59	
YTiO2.875	1.56	1.57	5.02	5.13	
YVO2.875	1.43	1.90	4.70	4.74	

Supplementary Electronic Density of States

Perfect structures with d electrons

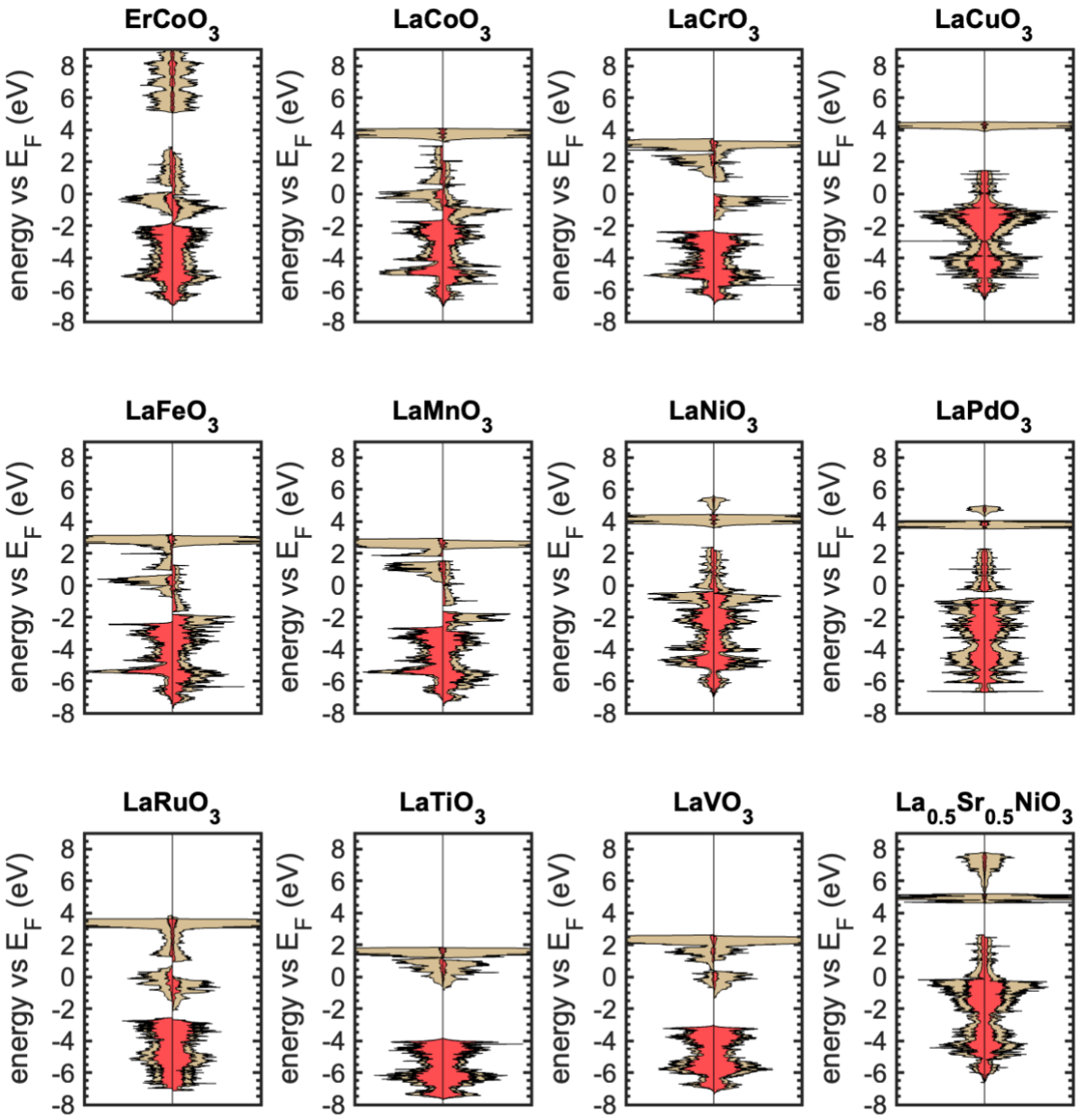

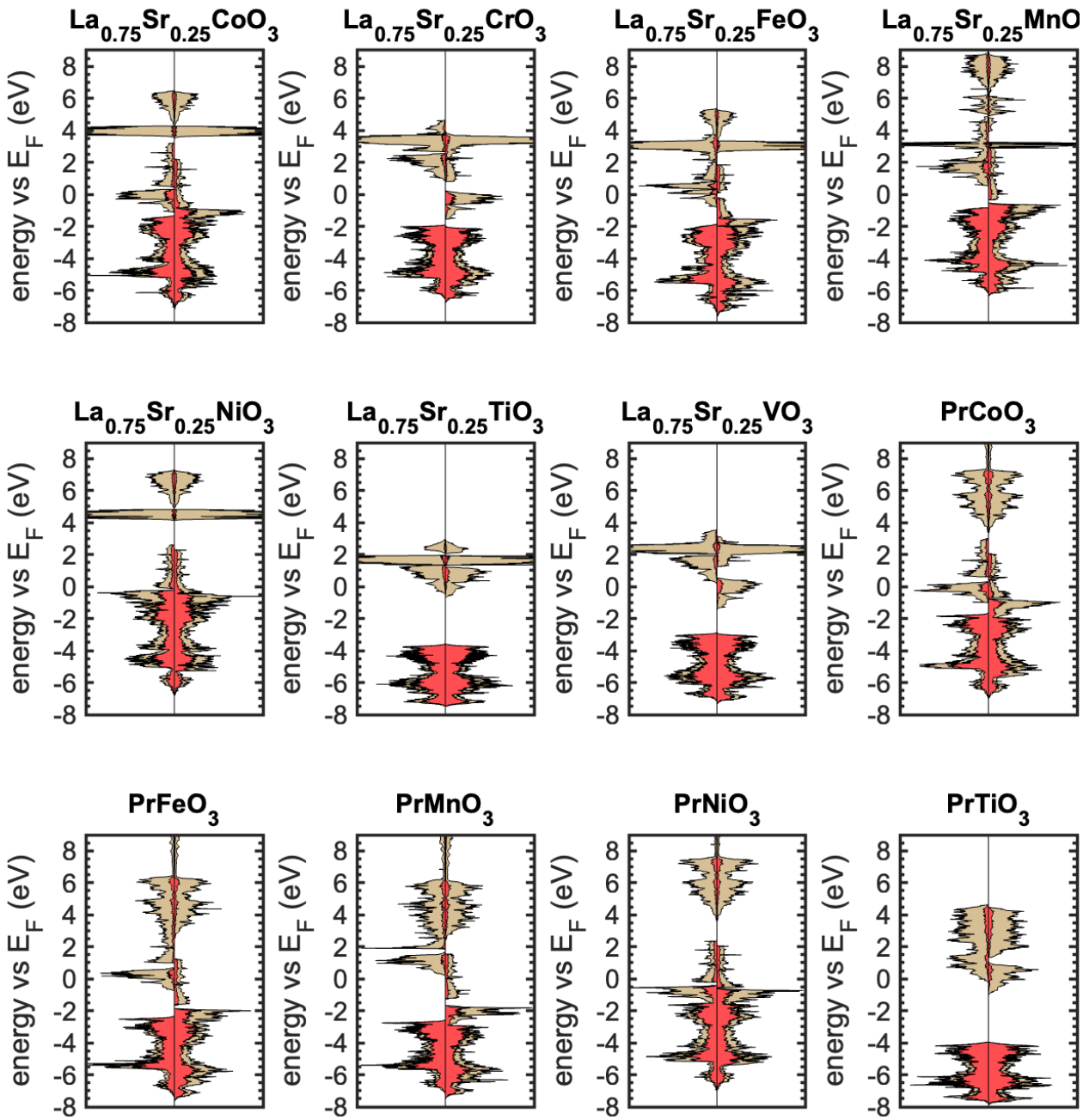
La0.75Sr0.25CoO3
La0.75Sr0.25CrO3
La0.75Sr0.25FeO3
La0.75Sr0.25MnO
La0.75Sr0.25NiO3
La0.75Sr0.25TiO3
La0.75Sr0.25VO3
PrCoO3
PrFeO3
PrMnO3
PrNiO3
PrTiO3
energy vs EF (eV)
8
6
4
2
0
-2
-4
-6
-8

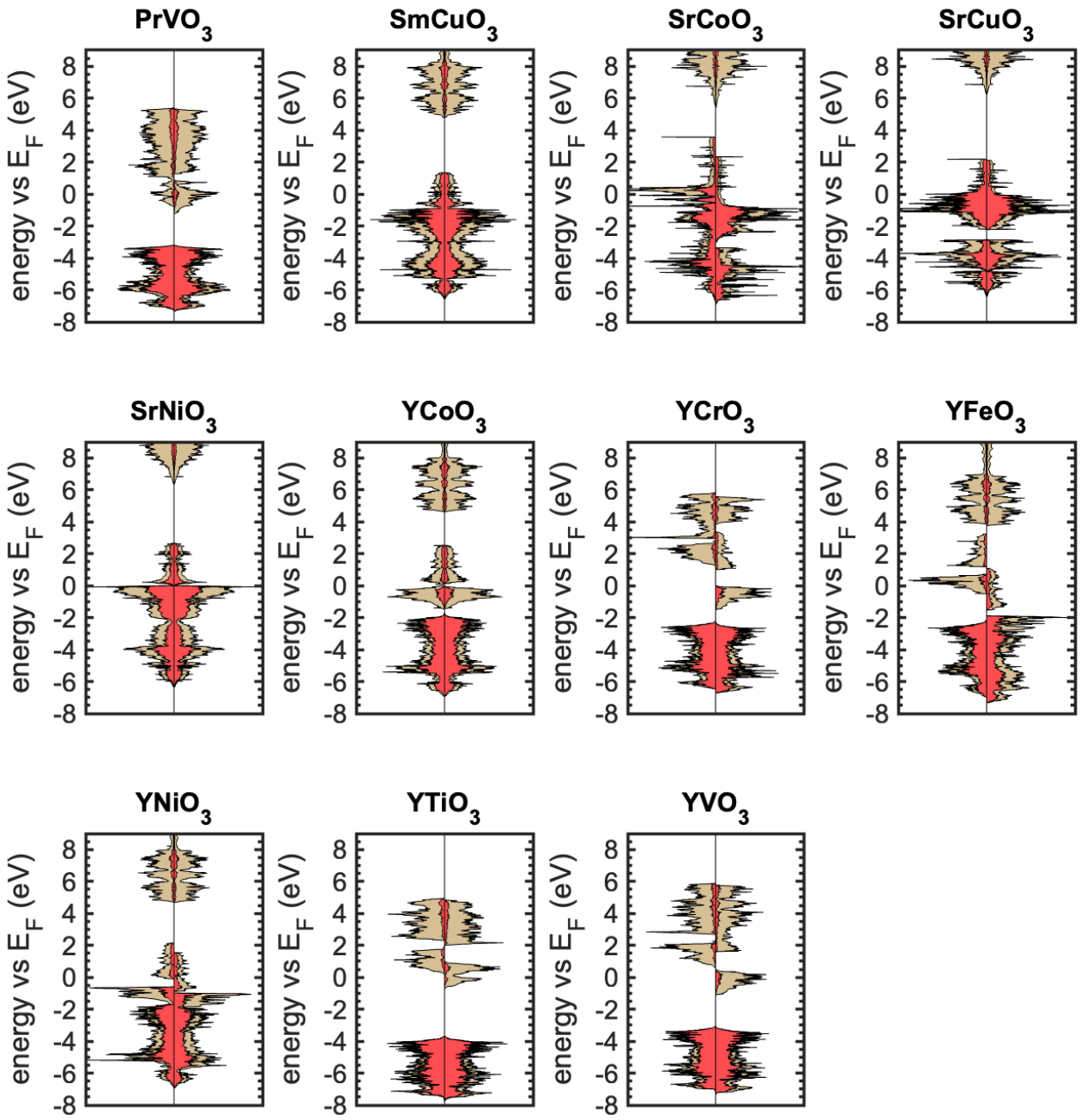
PrVO3
SmCuO3
SrCoO3
SrCuO3
SrNiO3
YCoO3
YCrO3
YFeO3
YNiO3
YTiO3
YVO3
energy vs EF (eV)
8
6
4
2
0
-2
-4
-6
-8

Perfect structures without d electrons

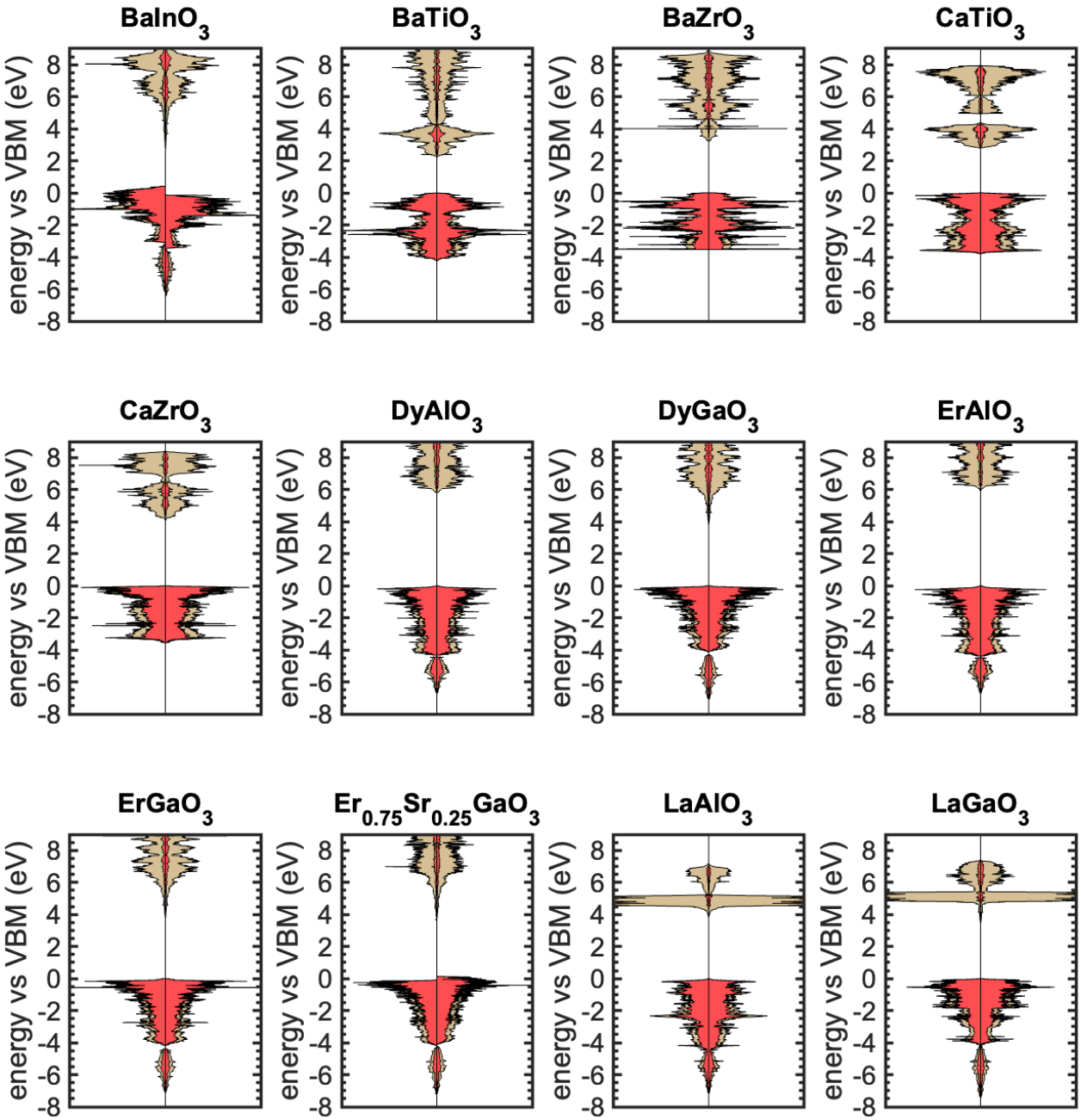

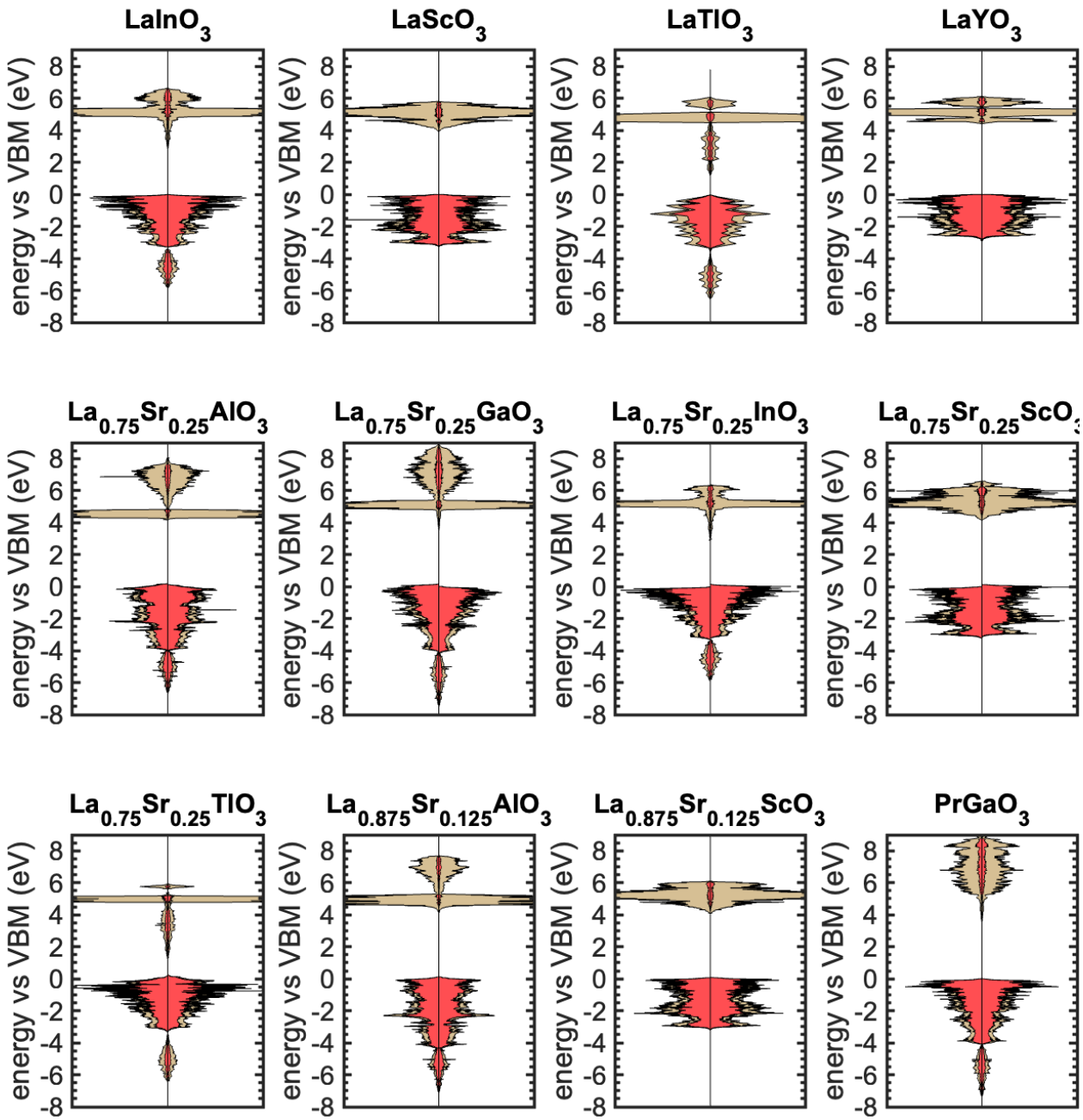
LaInO3
LaScO3
LaTlO3
LaYO3
La0.75Sr0.25AlO3
La0.75Sr0.25GaO3
La0.75Sr0.25InO3
La0.75Sr0.25ScO3
La0.75Sr0.25TlO3
La0.875Sr0.125AlO3
La0.875Sr0.125ScO3
PrGaO3
energy vs VBM (eV)
8
6
4
2
0
-2
-4
-6
-8

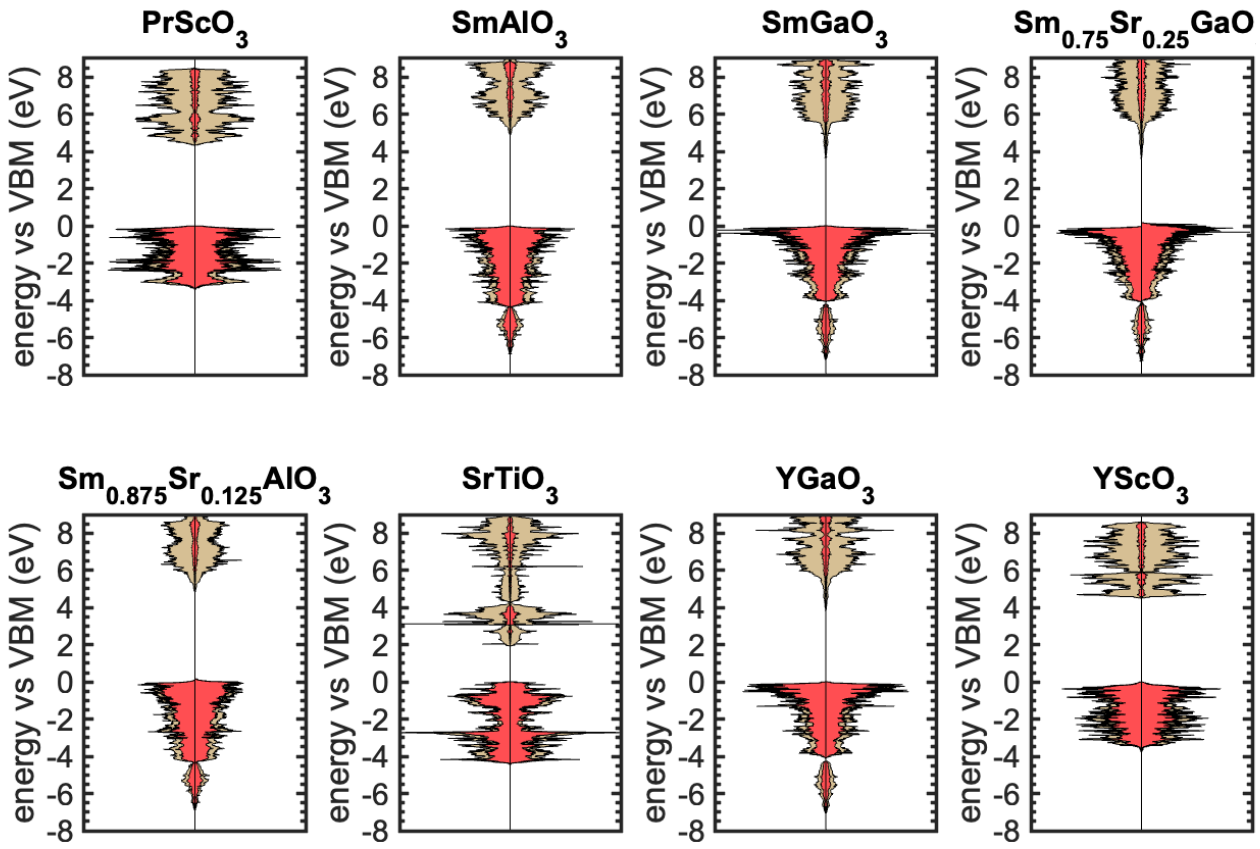
PrScO3
SmAlO3
SmGaO3
Sm0.75Sr0.25GaO
Sm0.875Sr0.125AlO3
SrTiO3
YGaO3
YScO3
energy vs VBM (eV)
8
6
4
2
0
-2
-4
-6
-8

NCC defected structures with d electrons

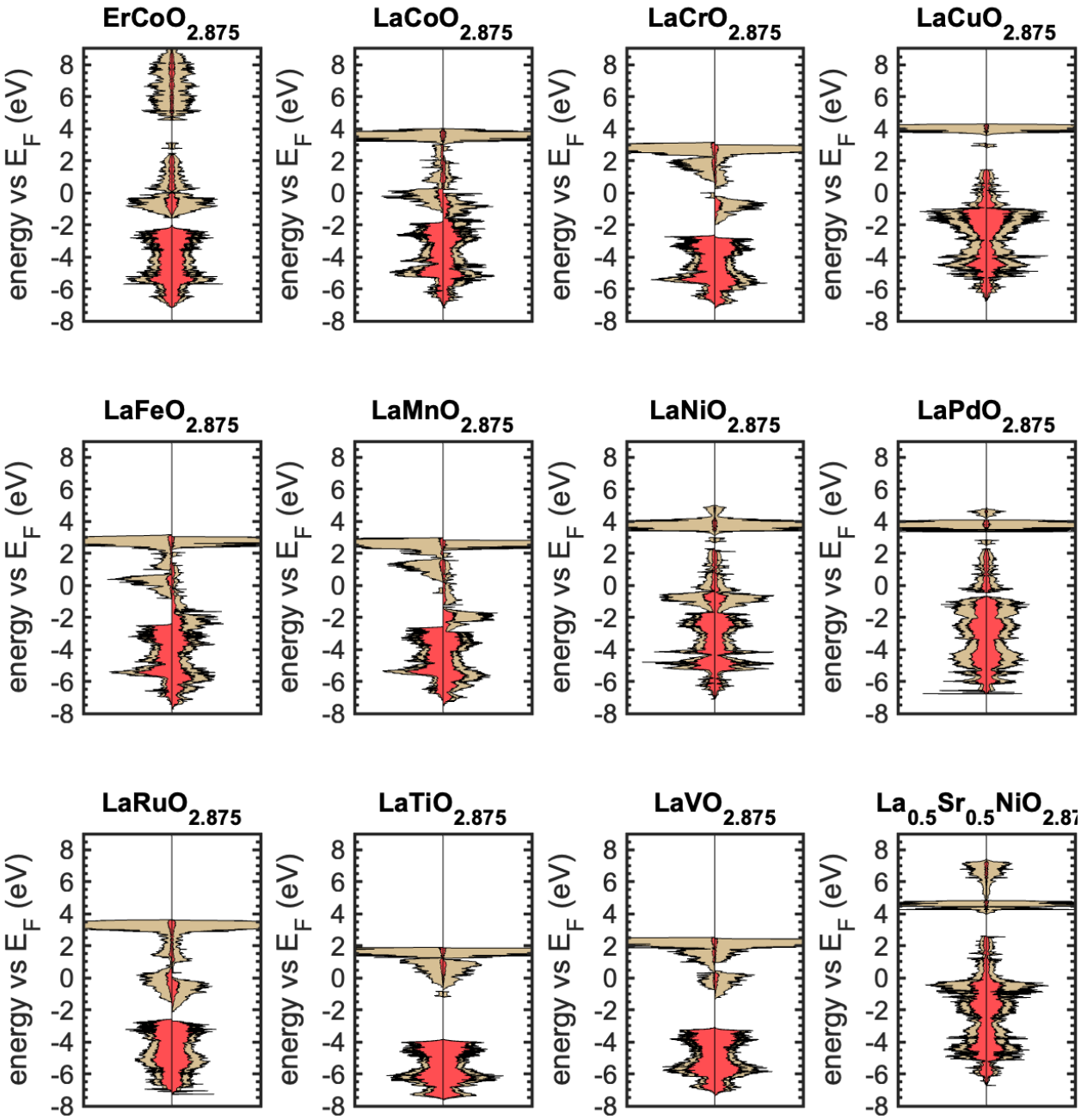

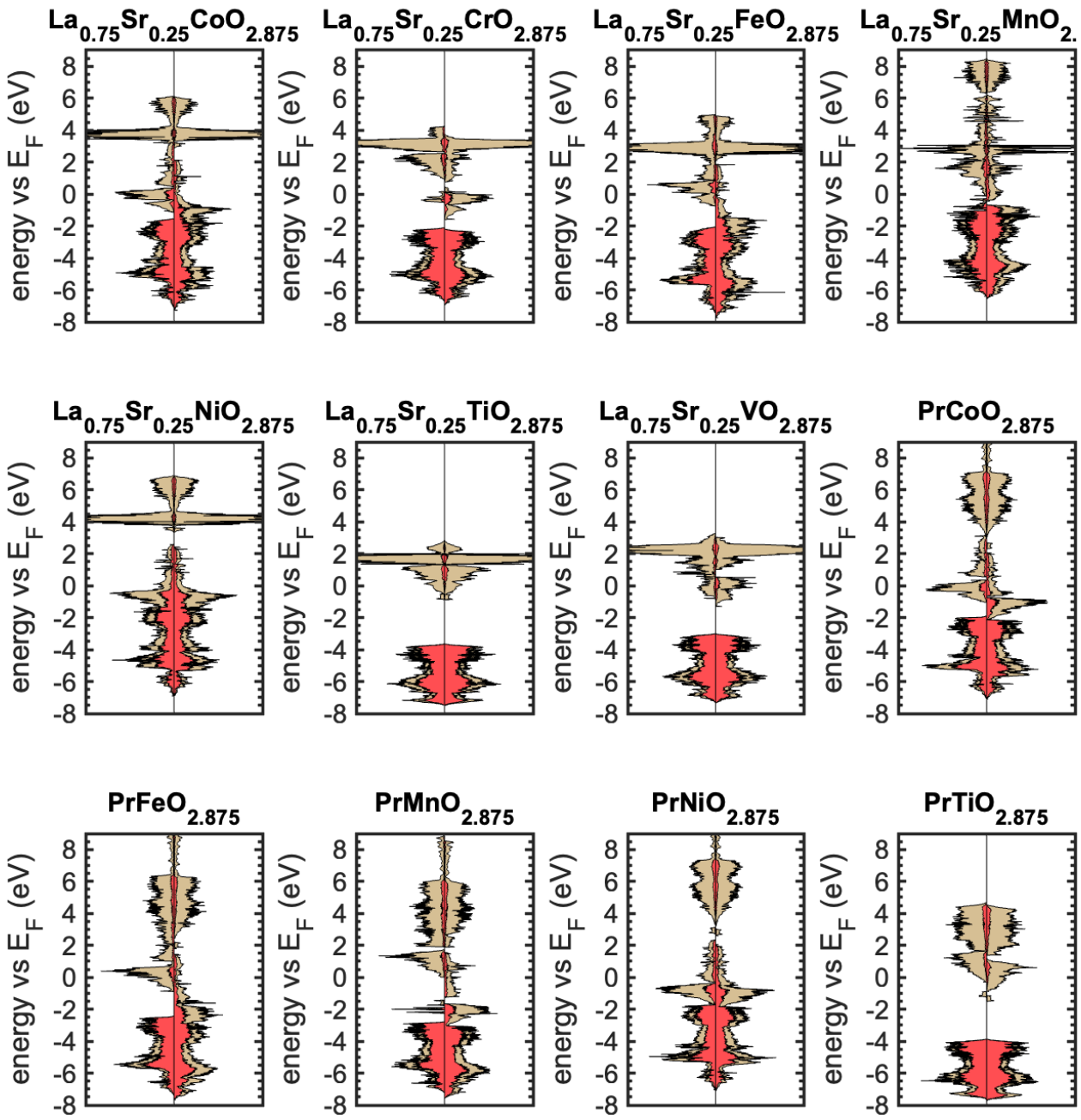
La0.75Sr0.25CoO2.875
La0.75Sr0.25CrO2.875
La0.75Sr0.25FeO2.875
La0.75Sr0.25MnO2.
La0.75Sr0.25NiO2.875
La0.75Sr0.25TiO2.875
La0.75Sr0.25VO2.875
PrCoO2.875
PrFeO2.875
PrMnO2.875
PrNiO2.875
PrTiO2.875
energy vs EF (eV)
8
6
4
2
0
-2
-4
-6
-8

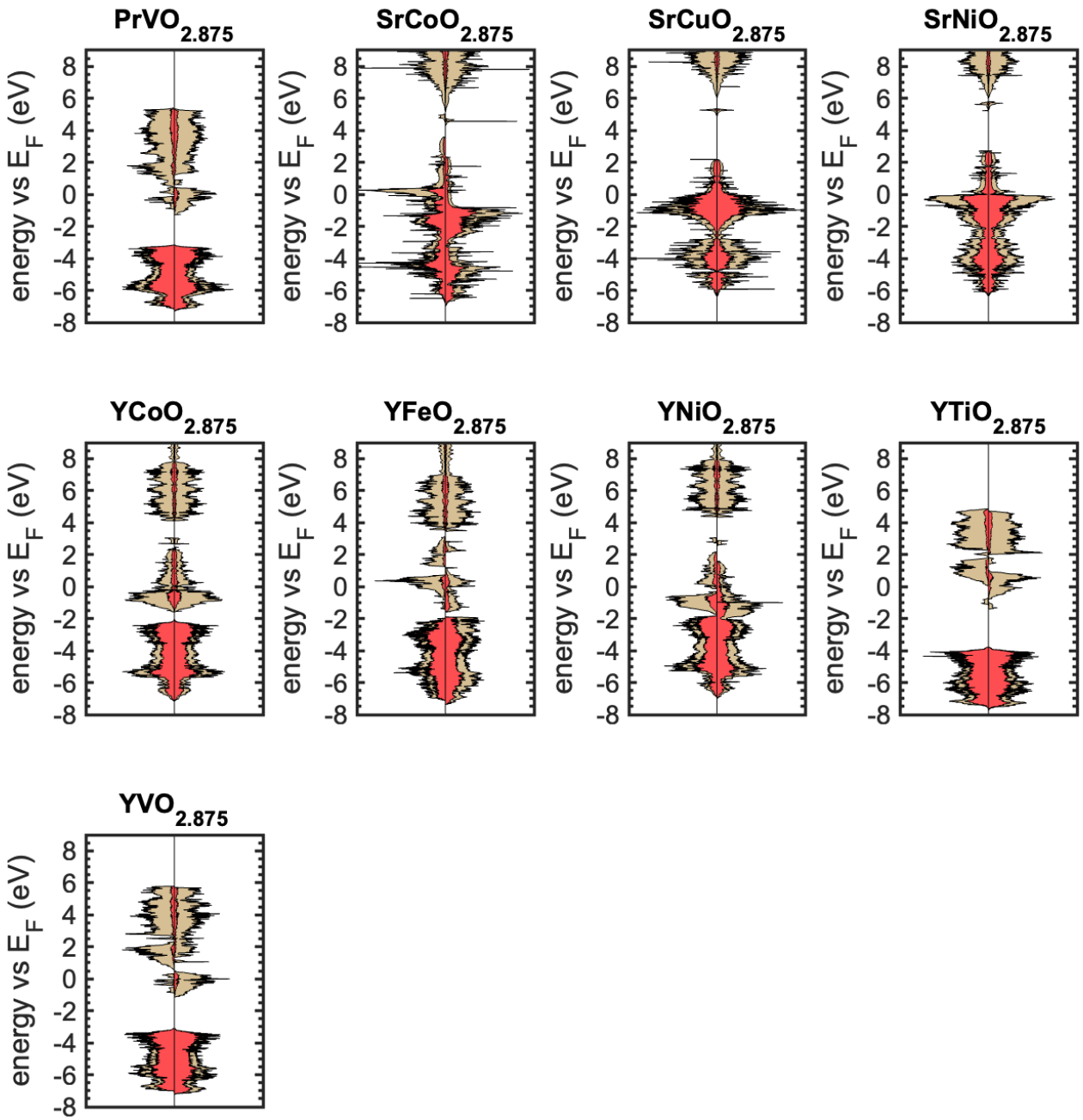
PrVO2.875
SrCoO2.875
SrCuO2.875
SrNiO2.875
YCoO2.875
YFeO2.875
YNiO2.875
YTiO2.875
YVO2.875
energy vs EF (eV)
8
6
4
2
0
-2
-4
-6
-8

CC defected structures with d electrons

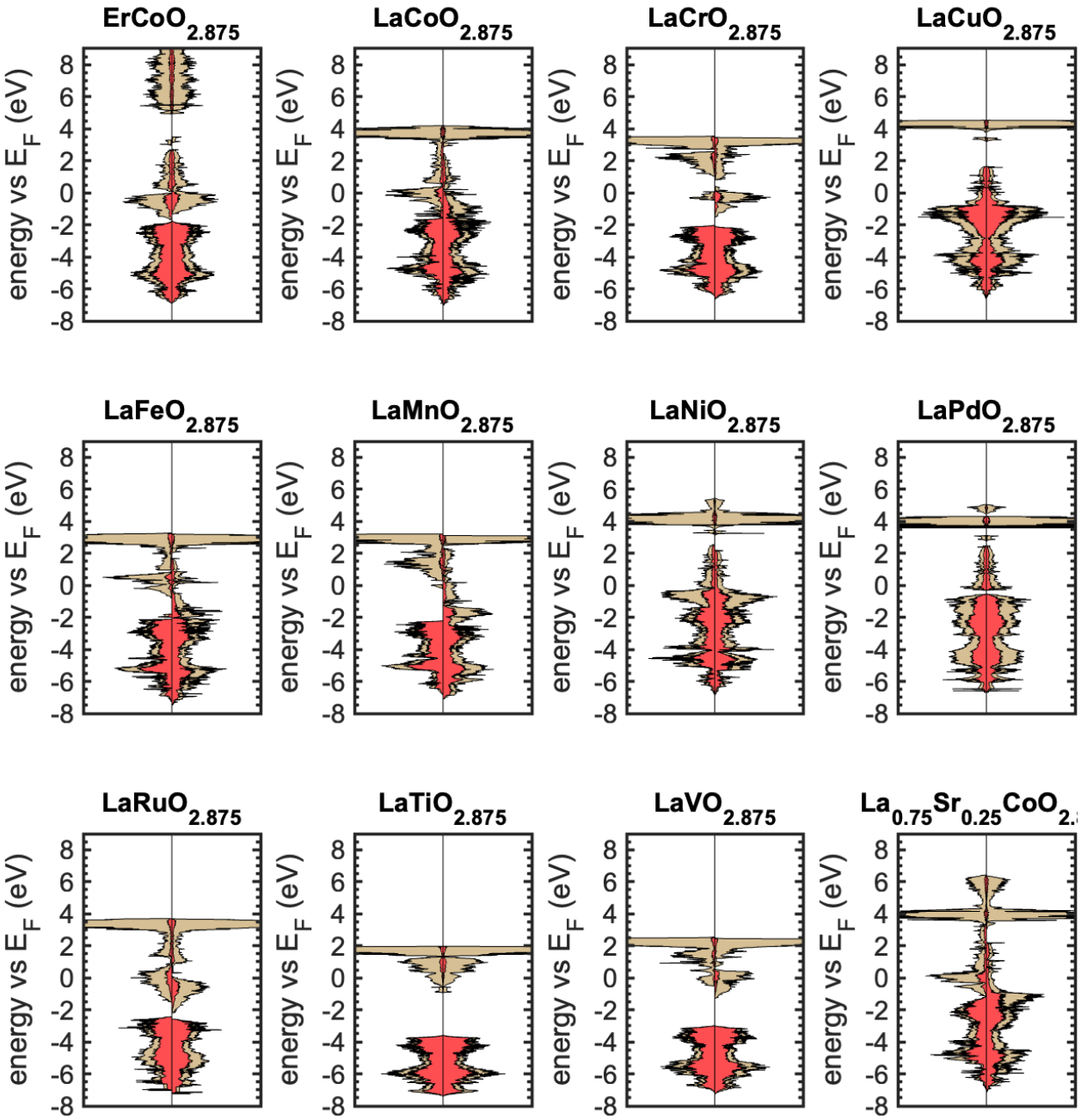

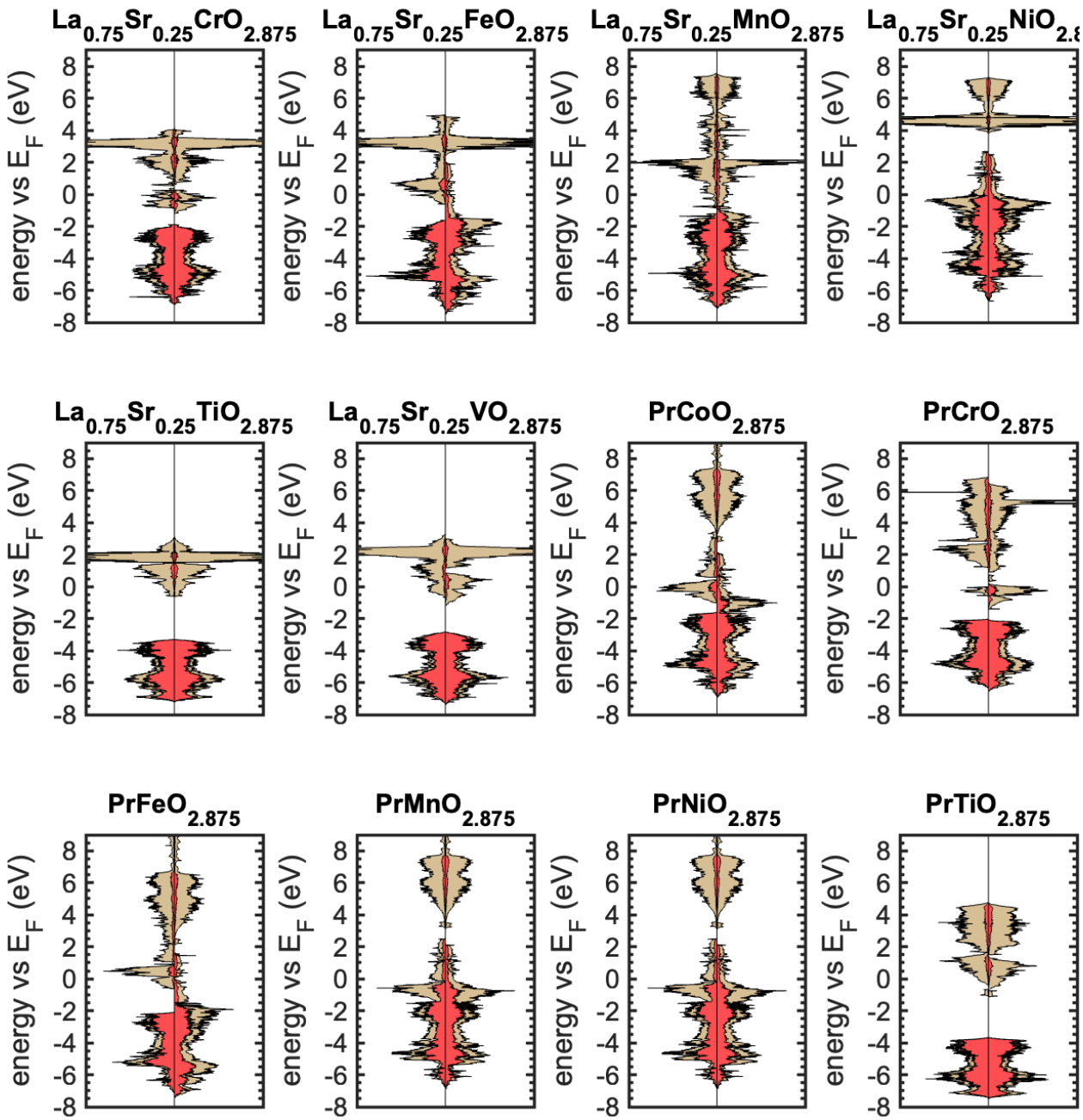
La0.75Sr0.25CrO2.875
La0.75Sr0.25FeO2.875
La0.75Sr0.25MnO2.875
La0.75Sr0.25NiO2.8
La0.75Sr0.25TiO2.875
La0.75Sr0.25VO2.875
PrCoO2.875
PrCrO2.875
PrFeO2.875
PrMnO2.875
PrNiO2.875
PrTiO2.875
energy vs EF (eV)
8
6
4
2
0
-2
-4
-6
-8

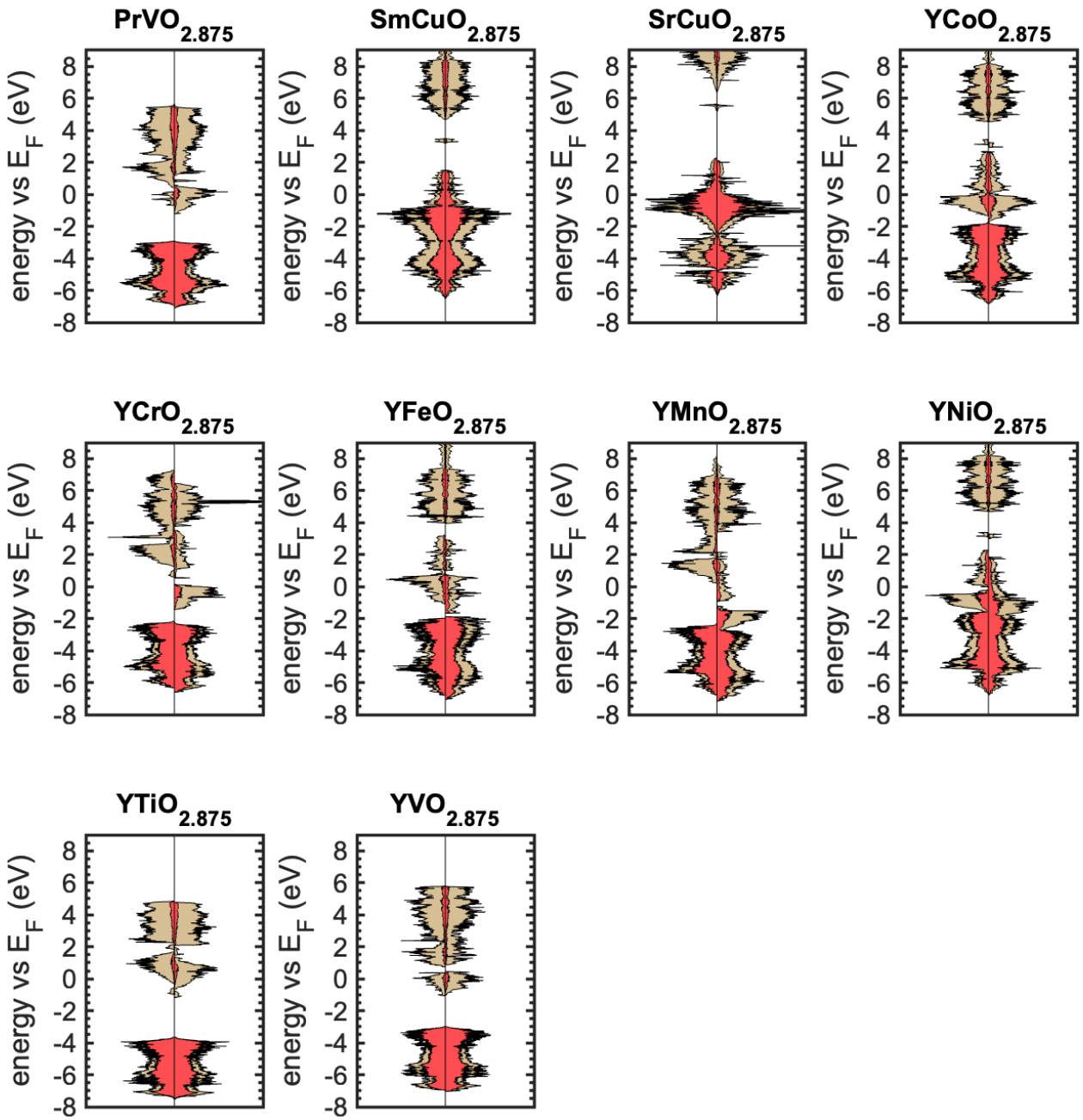
PrVO2.875
SmCuO2.875
SrCuO2.875
YCoO2.875
YCrO2.875
YFeO2.875
YMnO2.875
YNiO2.875
YTiO2.875
YVO2.875
energy vs EF (eV)
8
6
4
2
0
-2
-4
-6
-8

NCC defected structures without d electrons

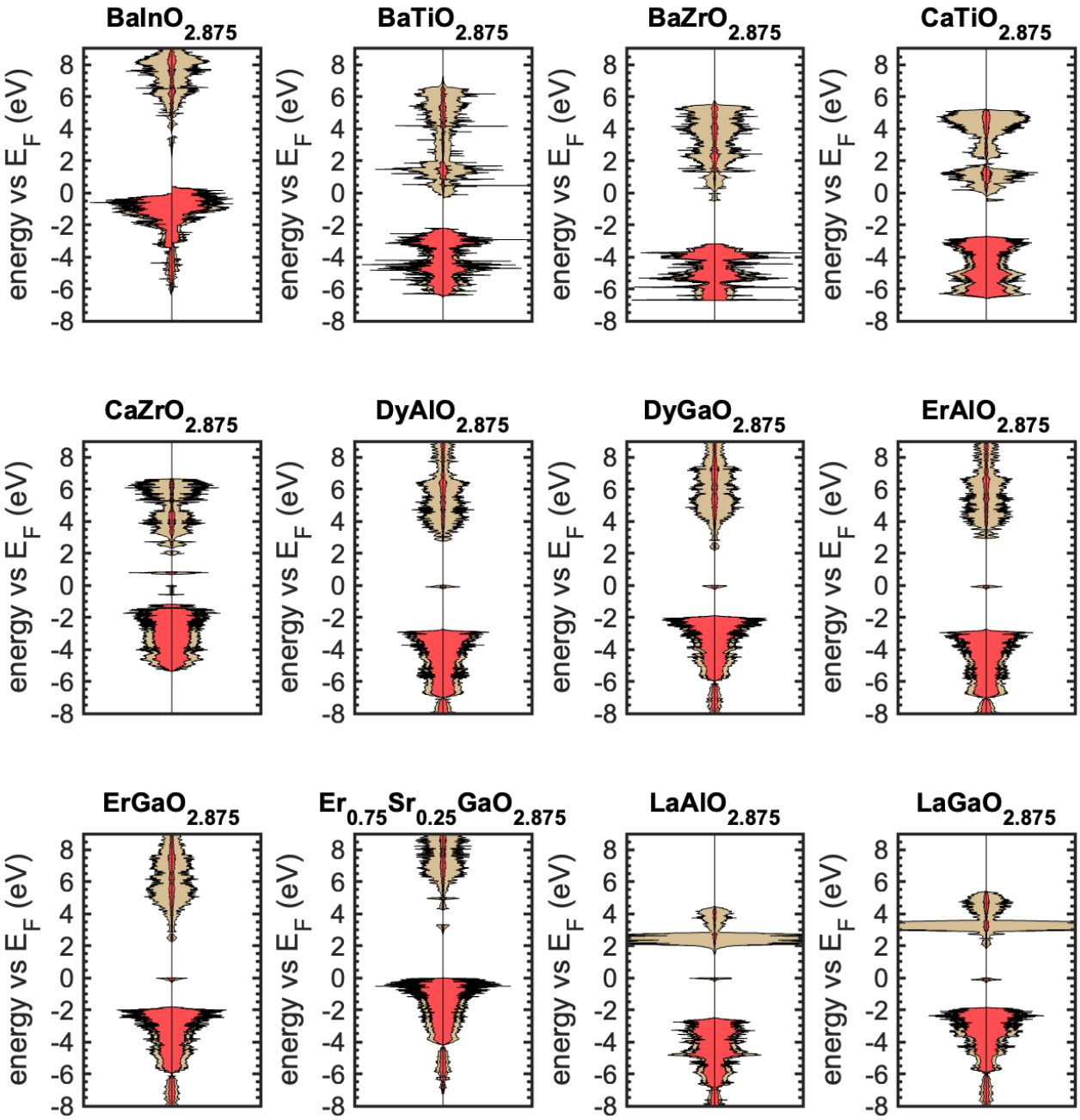

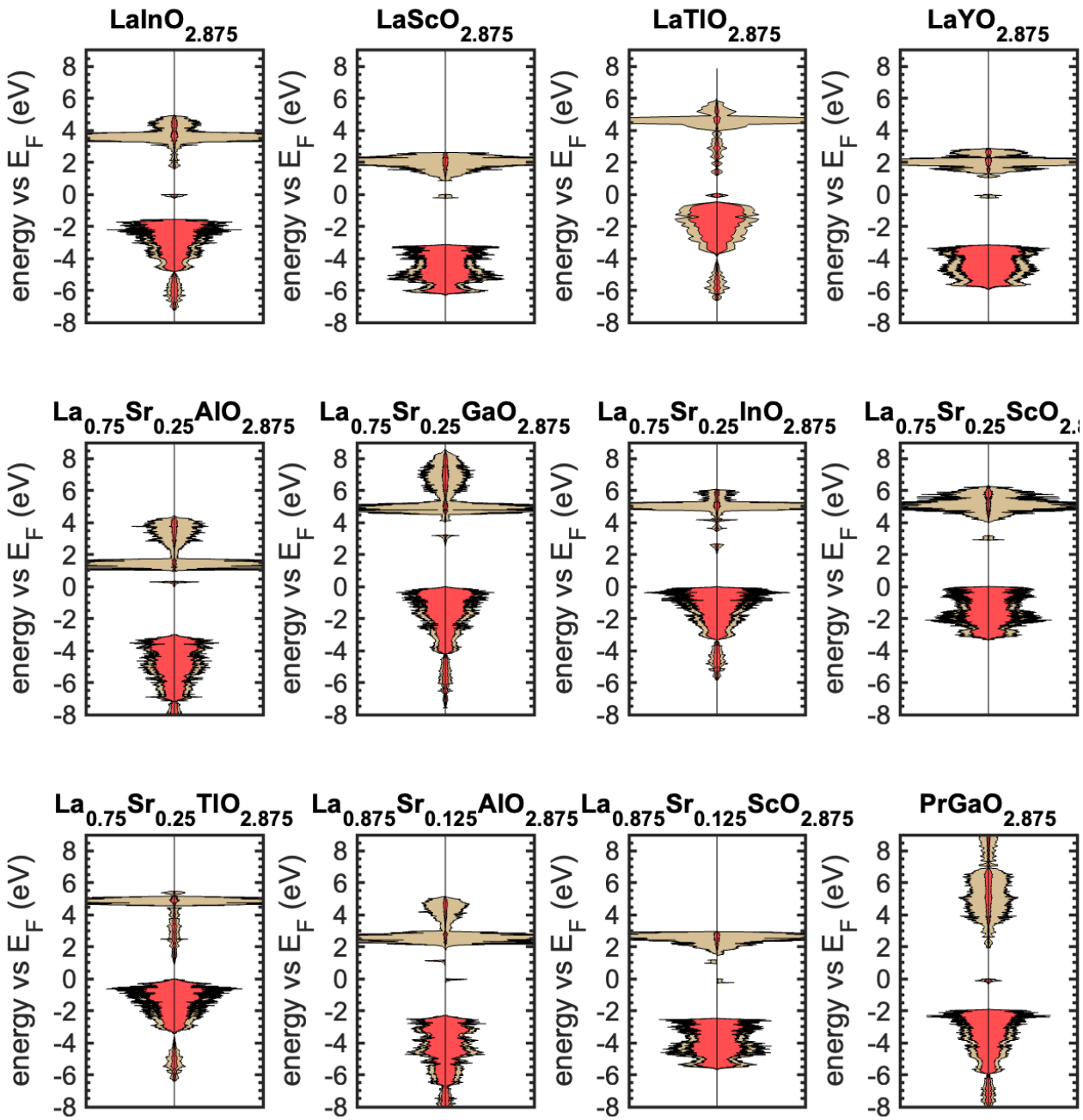
LaInO2.875
LaScO2.875
LaTlO2.875
LaYO2.875
La0.75Sr0.25AlO2.875
La0.75Sr0.25GaO2.875
La0.75Sr0.25InO2.875
La0.75Sr0.25ScO2.
La0.75Sr0.25TlO2.875
La0.875Sr0.125AlO2.875
La0.875Sr0.125ScO2.875
PrGaO2.875
energy vs EF (eV)
8
6
4
2
0
-2
-4
-6
-8

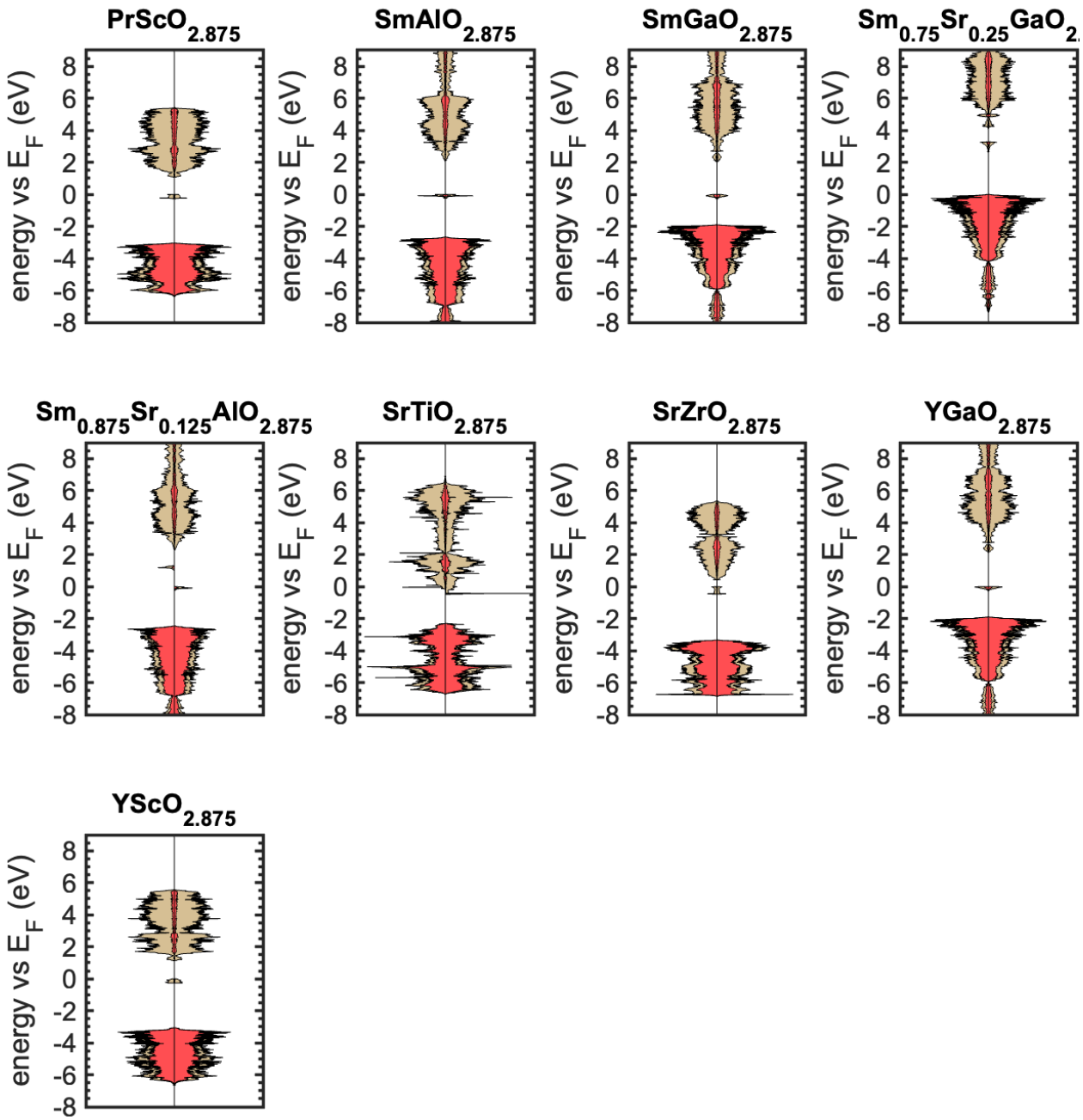
PrScO2.875
SmAlO2.875
SmGaO2.875
Sm0.75Sr0.25GaO2.
Sm0.875Sr0.125AlO2.875
SrTiO2.875
SrZrO2.875
YGaO2.875
YScO2.875
energy vs EF (eV)
8
6
4
2
0
-2
-4
-6
-8

CC defected structures without d electrons

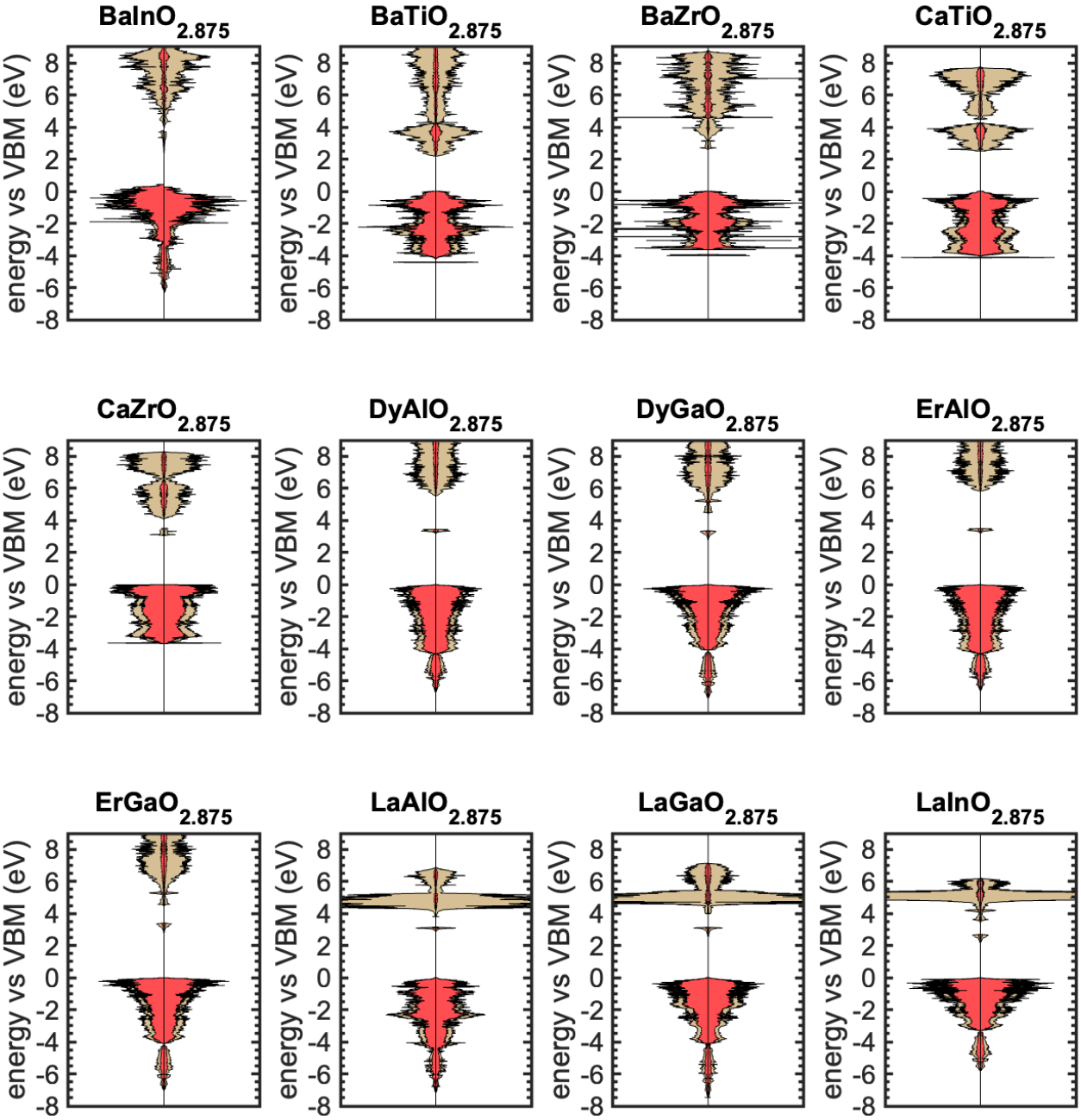

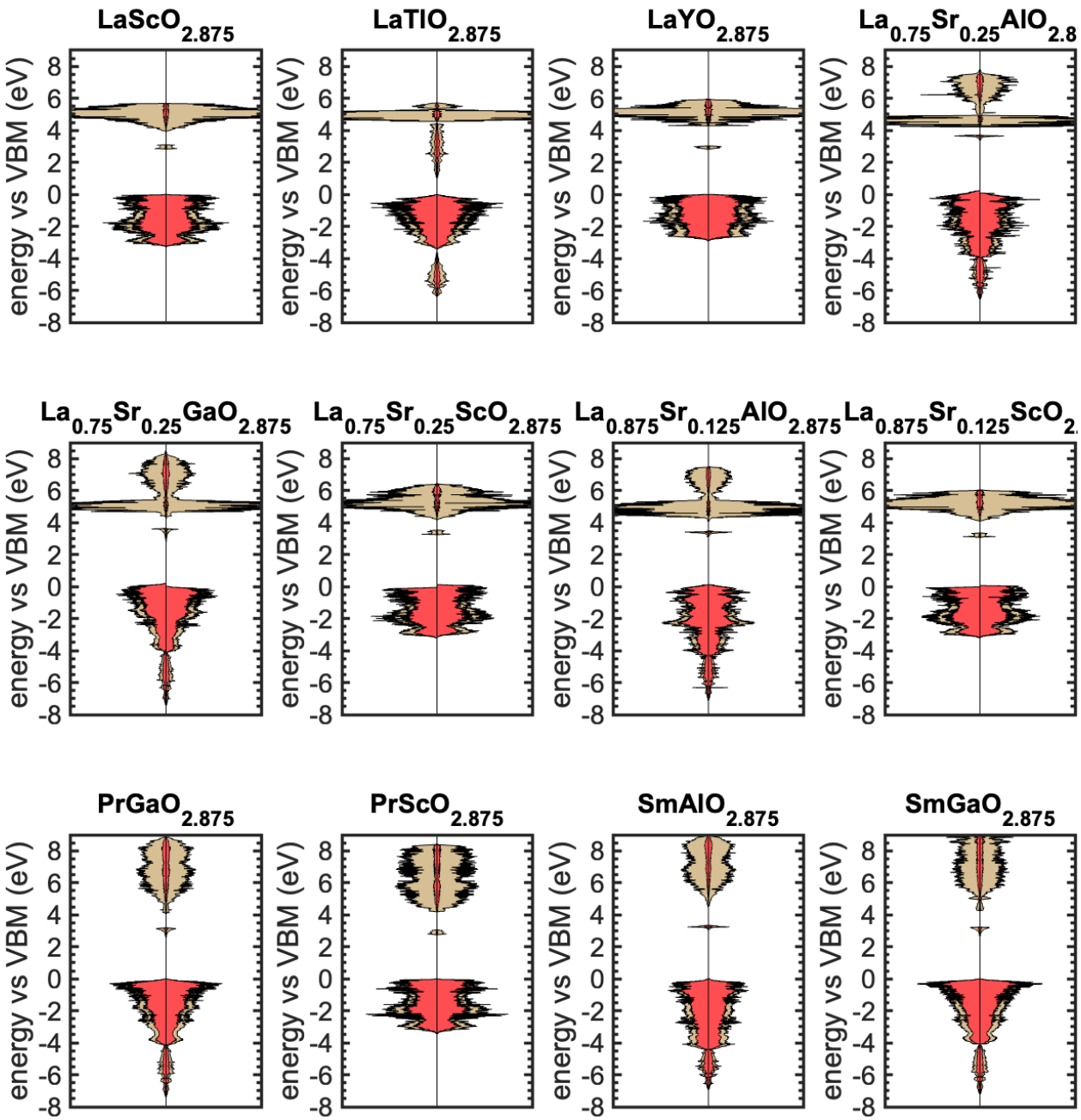
LaScO2.875
LaTlO2.875
LaYO2.875
La0.75Sr0.25AlO2.8
La0.75Sr0.25GaO2.875
La0.75Sr0.25ScO2.875
La0.875Sr0.125AlO2.875
La0.875Sr0.125ScO2.
PrGaO2.875
PrScO2.875
SmAlO2.875
SmGaO2.875
energy vs VBM (eV)
8
6
4
2
0
-2
-4
-6
-8

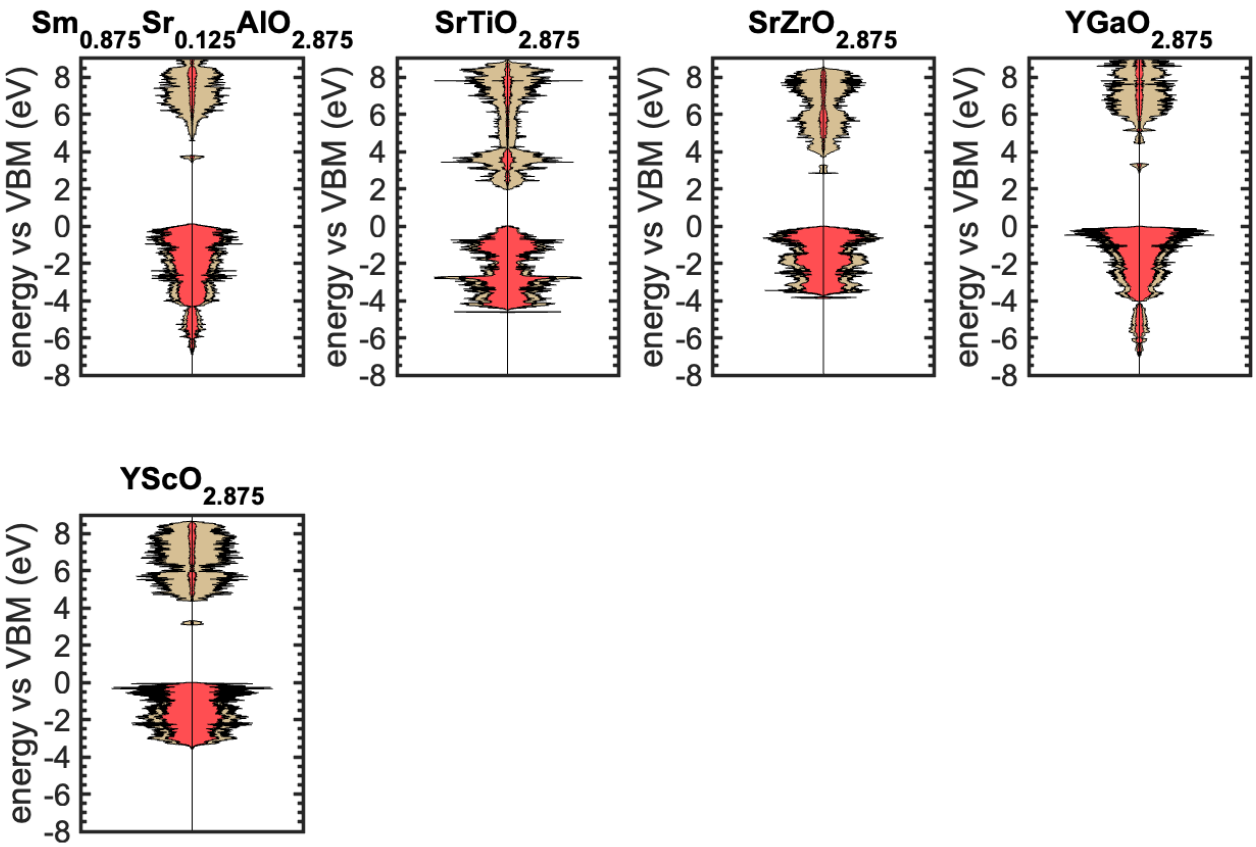
Sm0.875Sr0.125AlO2.875
SrTiO2.875
SrZrO2.875
YGaO2.875
YScO2.875
energy vs VBM (eV)
8
6
4
2
0
-2
-4
-6
-8

NCC defected structures without d electrons – Transition State

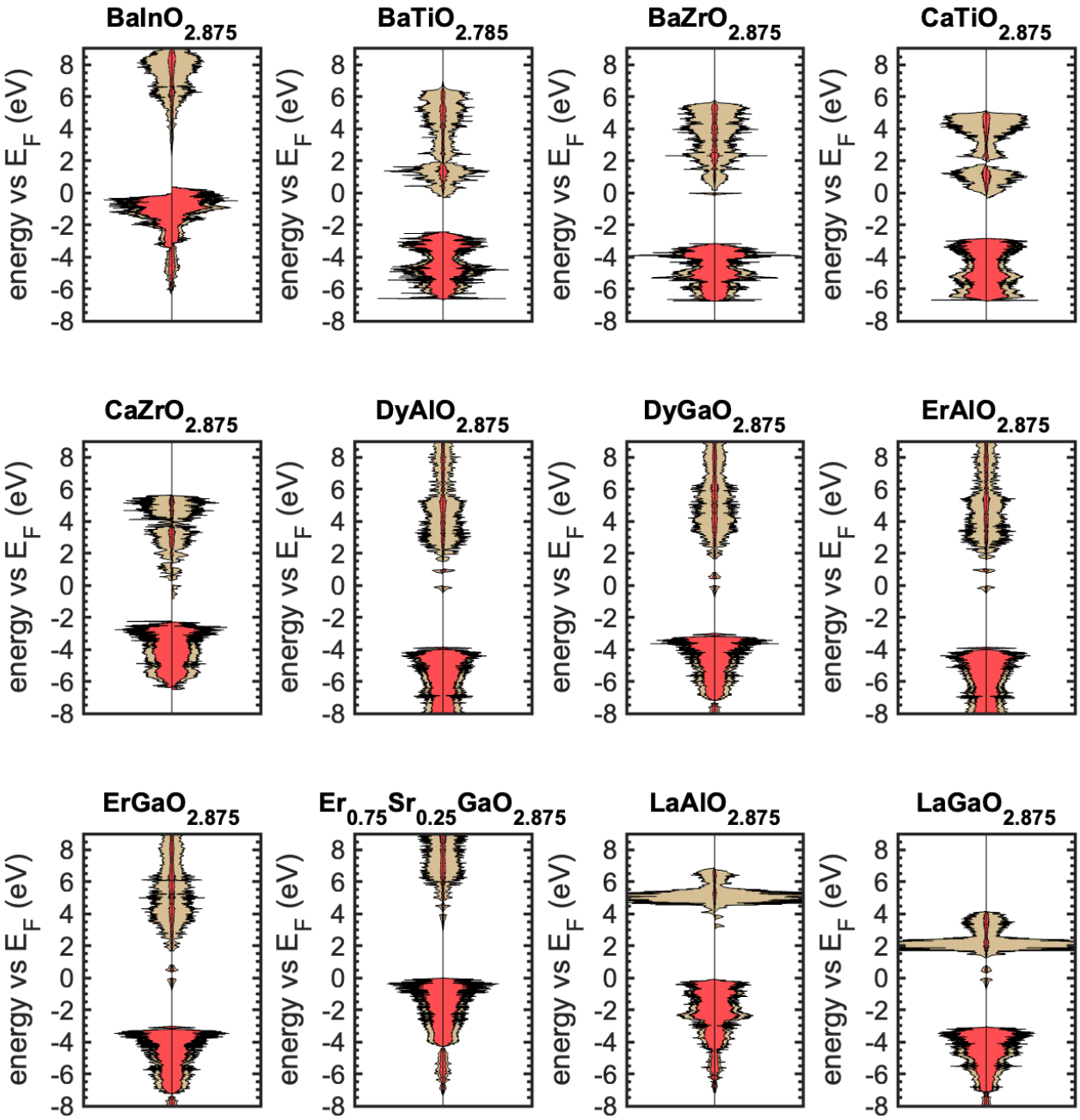

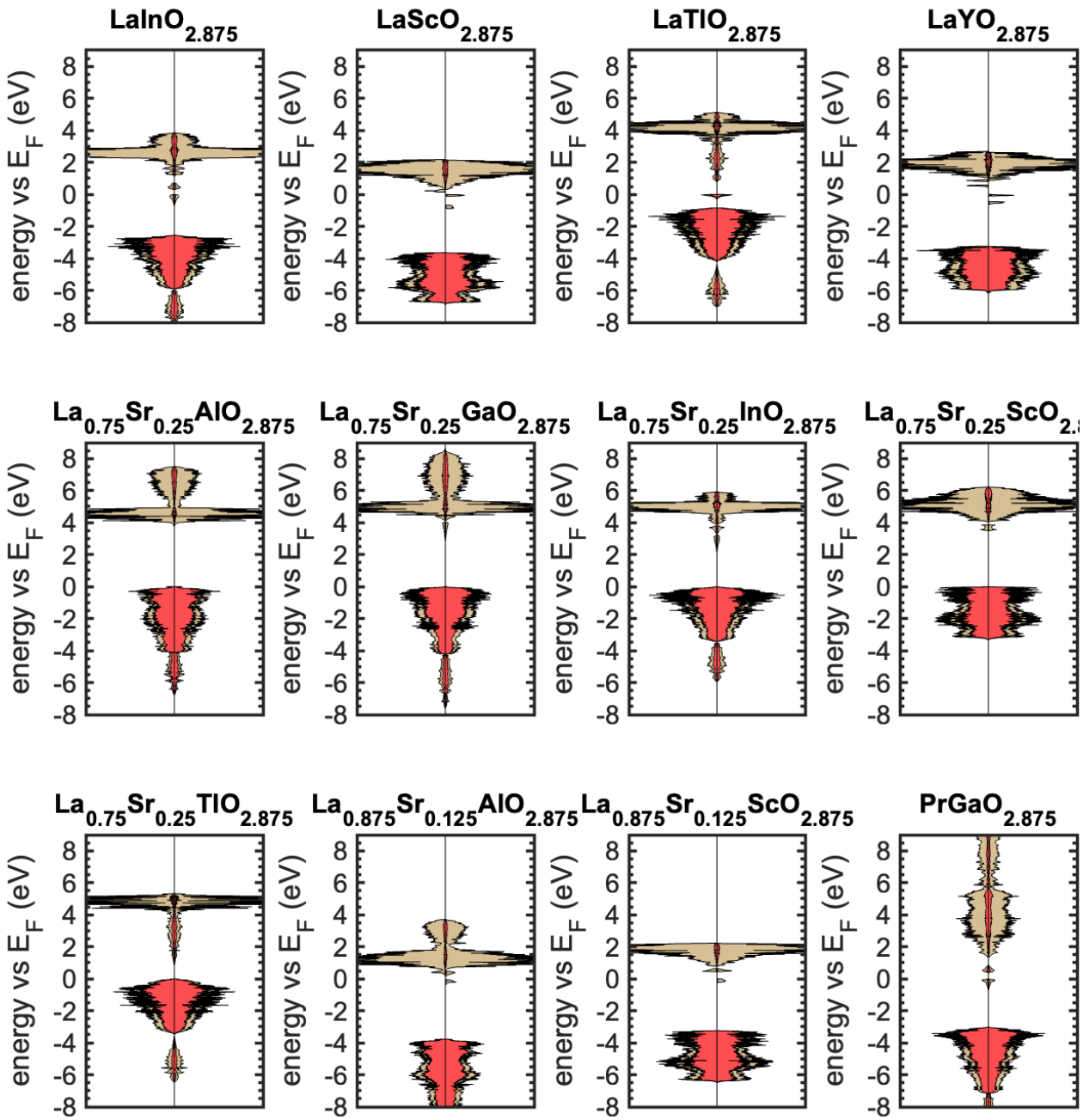
LaInO2.875
LaScO2.875
LaTlO2.875
LaYO2.875
La0.75Sr0.25AlO2.875
La0.75Sr0.25GaO2.875
La0.75Sr0.25InO2.875
La0.75Sr0.25ScO2.
La0.75Sr0.25TlO2.875
La0.875Sr0.125AlO2.875
La0.875Sr0.125ScO2.875
PrGaO2.875
energy vs EF (eV)
8
6
4
2
0
-2
-4
-6
-8

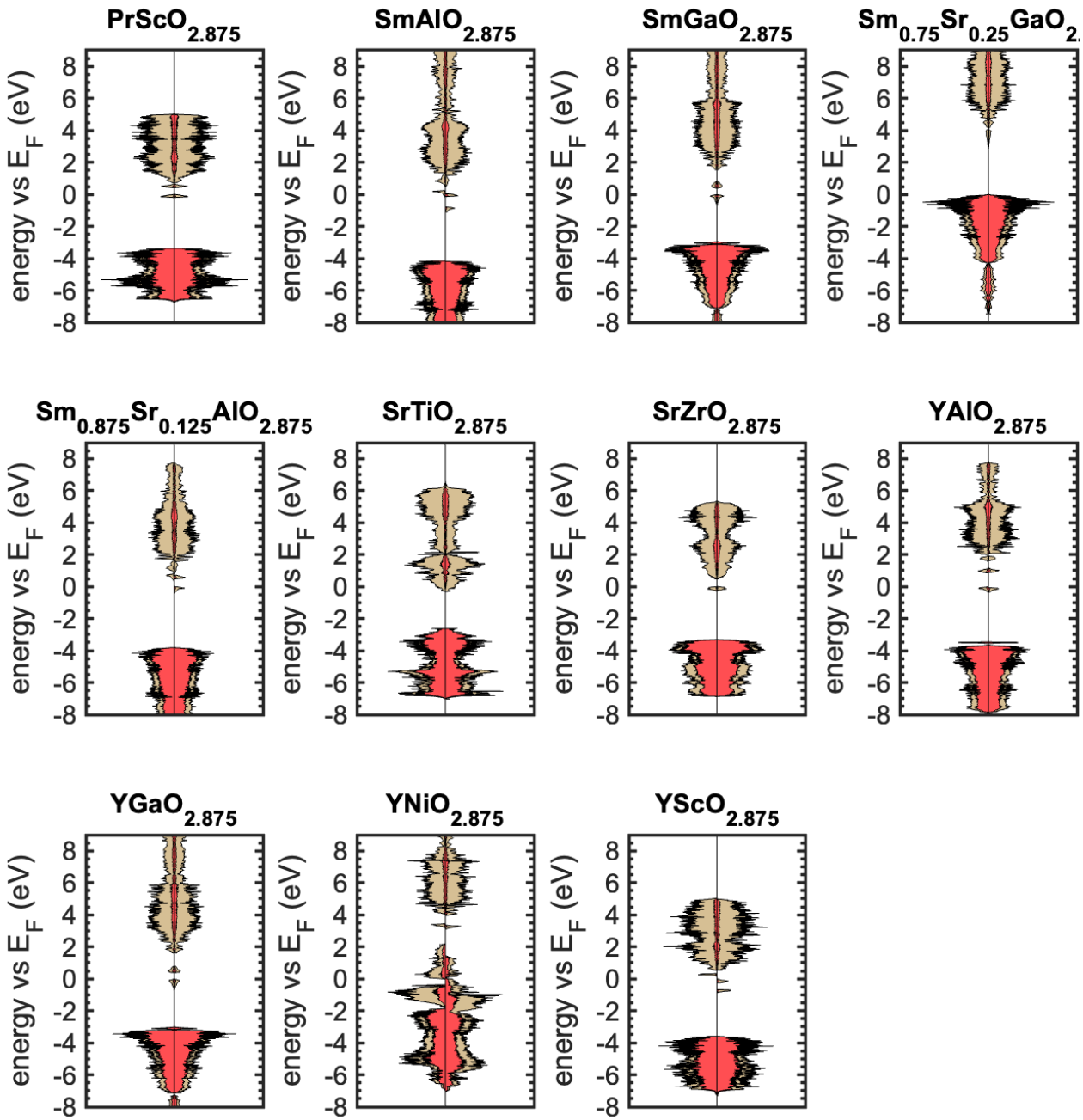
PrScO2.875
SmAlO2.875
SmGaO2.875
Sm0.75Sr0.25GaO2
Sm0.875Sr0.125AlO2.875
SrTiO2.875
SrZrO2.875
YAlO2.875
YGaO2.875
YNiO2.875
YScO2.875
energy vs EF (eV)
8
6
4
2
0
-2
-4
-6
-8

CC defected structures without d electrons – Transition State

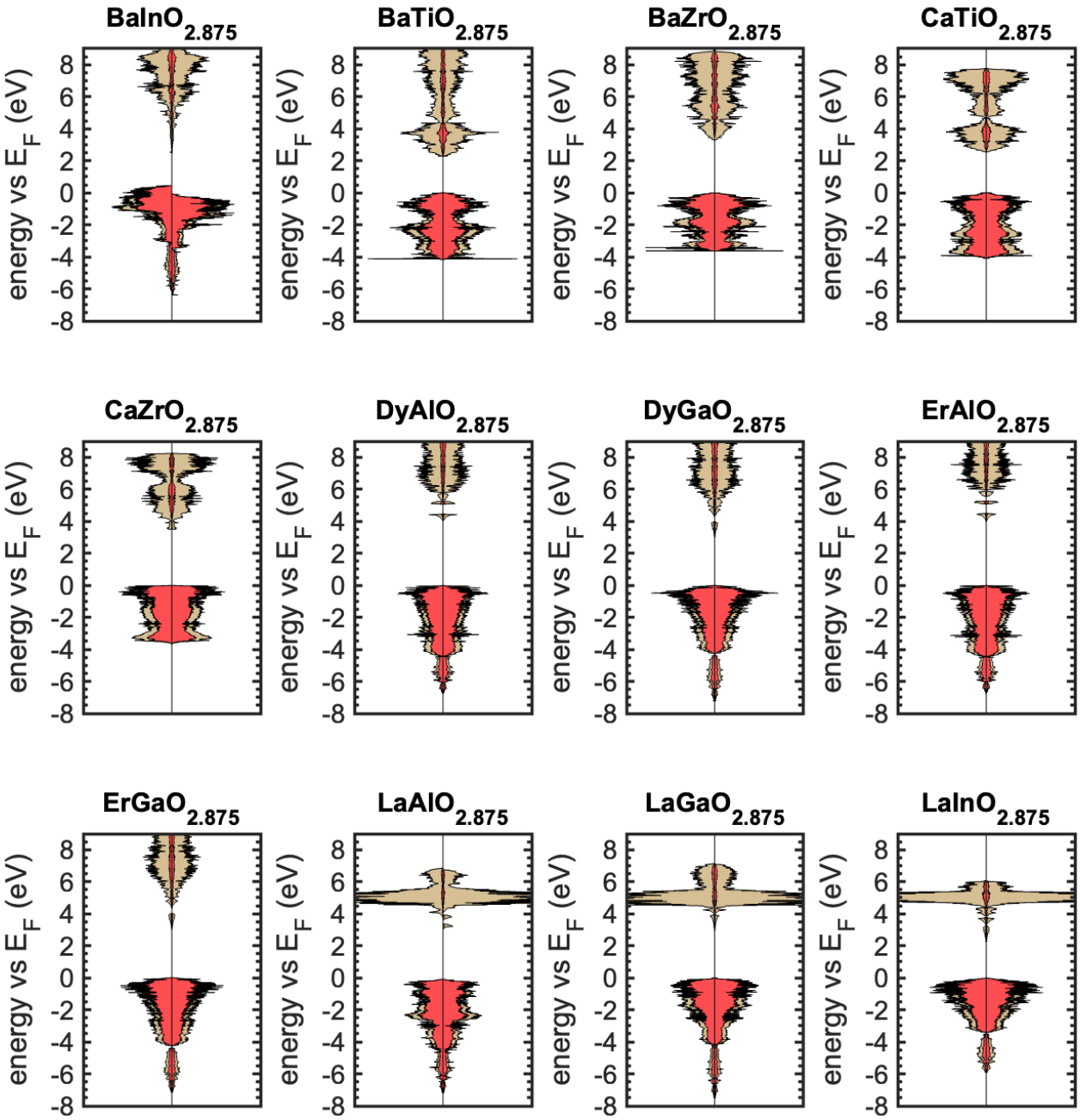

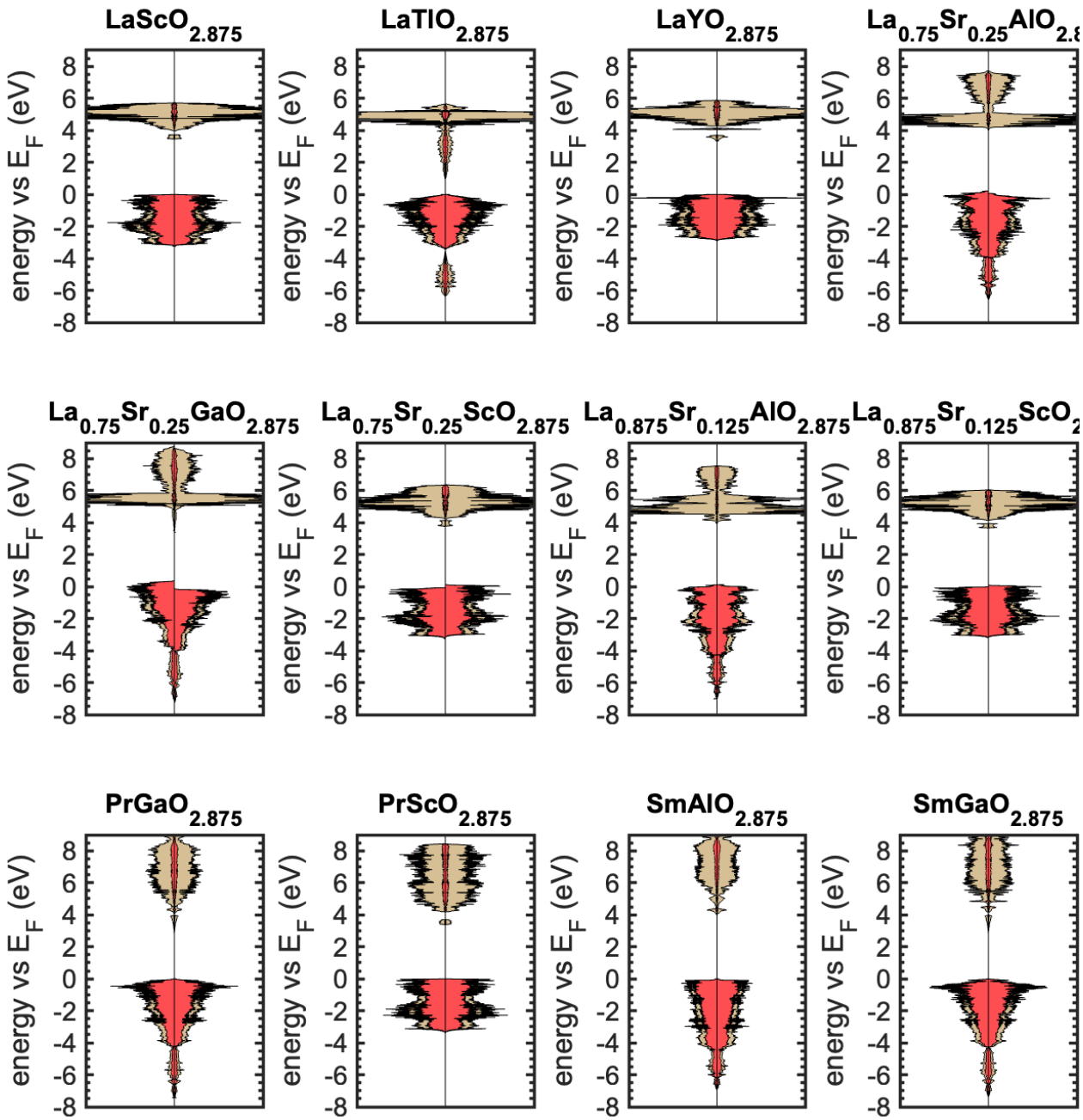
LaScO2.875
LaTlO2.875
LaYO2.875
La0.75Sr0.25AlO2.8
La0.75Sr0.25GaO2.875
La0.75Sr0.25ScO2.875
La0.875Sr0.125AlO2.875
La0.875Sr0.125ScO2
PrGaO2.875
PrScO2.875
SmAlO2.875
SmGaO2.875
energy vs EF (eV)
8
6
4
2
0
-2
-4
-6
-8

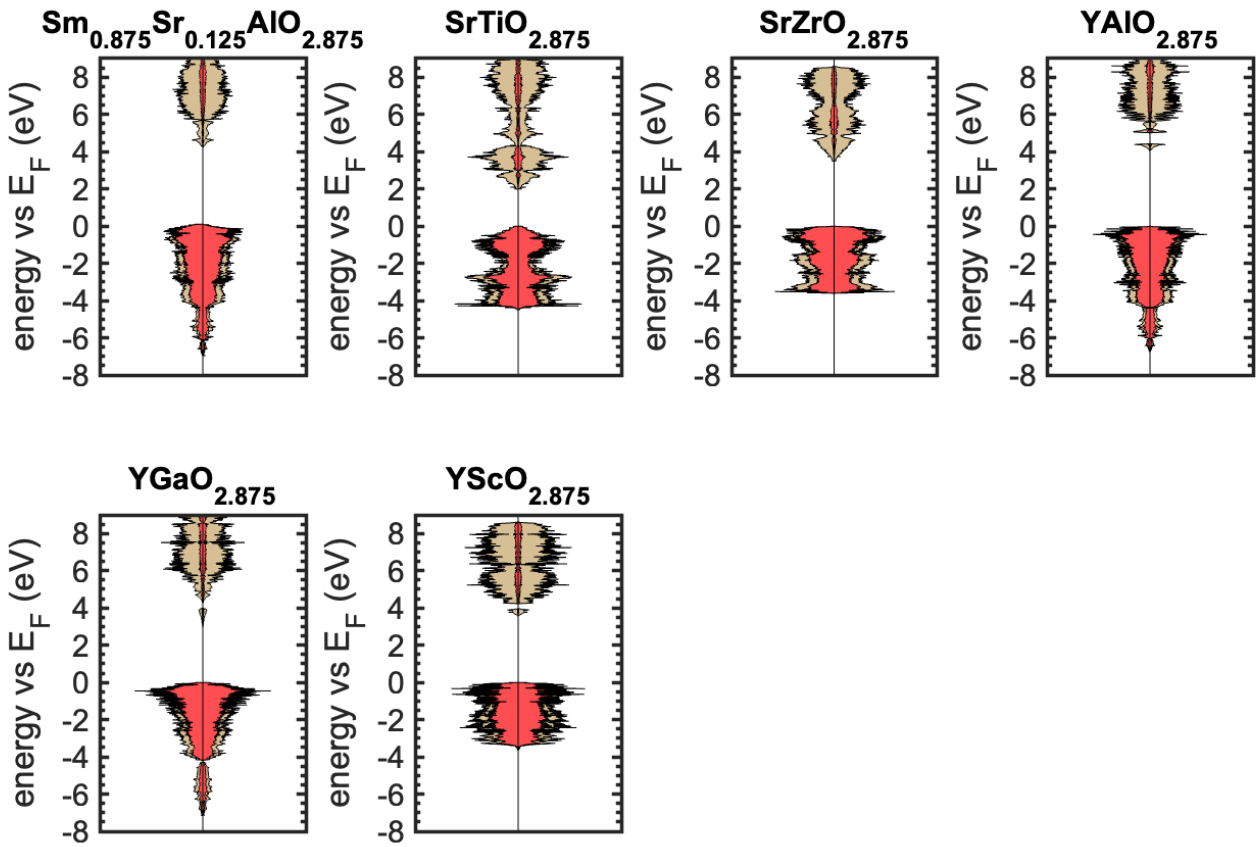
Sm0.875Sr0.125AlO2.875
SrTiO2.875
SrZrO2.875
YAlO2.875
YGaO2.875
YScO2.875
energy vs EF (eV)
8
6
4
2
0
-2
-4
-6
-8

Supplemental References

1. Freysoldt, C. *et al.* First-principles calculations for point defects in solids. *Rev Mod Phys* **86**, 253–305 (2014).
2. Goyal, A., Gorai, P., Peng, H., Lany, S. & Stevanović, V. A computational framework for automation of point defect calculations. *Comput Mater Sci* **130**, 1–9 (2017).
3. Lany, S. & Zunger, A. Assessment of correction methods for the band-gap problem and for finite-size effects in supercell defect calculations: Case studies for ZnO and GaAs. *Phys Rev B* **78**, 235104 (2008).
4. Henkelman, G., Arnaldsson, A. & Jónsson, H. A fast and robust algorithm for Bader decomposition of charge density. *Comput Mater Sci* **36**, 354–360 (2006).
5. Ishigaki, T., Yamauchi, S., Kishio, K., Mizusaki, J. & Fueki, K. Diffusion of oxide ion vacancies in perovskite-type oxides. *J Solid State Chem* **73**, 179–187 (1988).
6. Belzner, A., Gür, T. M. & Huggins, R. A. Oxygen chemical diffusion in strontium doped lanthanum manganites. *Solid State Ion* **57**, 327–337 (1992).
7. Yasuda, I., Ogasawara, K. & Hishinuma, M. Oxygen tracer diffusion in polycrystalline calcium-doped lanthanum chromites. *Journal of the American Ceramic Society* **80**, 3009–3012 (1997).
8. Nomura, K. & Tanase, S. Electrical conduction behavior in (La0.9Sr0.1)MIIIO3-δ (MIII = Al, Ga, Sc, In, and Lu) perovskites. *Solid State Ion* **98**, 229–236 (1997).
9. De Souza, R. A., Metlenko, V., Park, D. & Weirich, T. E. Behavior of oxygen vacancies in single-crystal SrTiO 3: Equilibrium distribution and diffusion kinetics. *Phys Rev B Condens Matter Mater Phys* **85**, 1–11 (2012).
10. Kessel, M., De Souza, R. A. & Martin, M. Oxygen diffusion in single crystal barium titanate. *Physical Chemistry Chemical Physics* **17**, 12587–12597 (2015).
11. Hayward, S. A. *et al.* Transformation processes in la al o 3: Neutron diffraction, dielectric, thermal, optical, and raman studies. *Phys Rev B* **72**, 054110 (2005).
12. Takahashi, T. & Iwahara, H. Ionic conduction in perovskite-type oxide solid solution and its application to the solid electrolyte fuel cell. *Energy Conversion* **11**, 105–111 (1971).
13. Chen, T.-Y. & Fung, K.-Z. Comparison of dissolution behavior and ionic conduction between Sr and/or Mg doped LaGaO3 and LaAlO3. *J Power Sources* **132**, 1–10 (2004).
14. Kilner, J. A. & Brook, R. J. A study of oxygen ion conductivity in doped non-stoichiometric oxides. *Solid State Ion* **6**, 237–252 (1982).
15. Ishihara, T. *et al.* Oxide Ion Conductivity in Doubly Doped PrGaO3 Perovskite-Type Oxide. *J Electrochem Soc* **146**, 1643 (1999).
16. Mayeshiba, T. T. & Morgan, D. D. Factors controlling oxygen migration barriers in perovskites. *Solid State Ion* **296**, 71–77 (2016).
17. Zheng, Y.-S. *et al.* Electronic origin of oxygen transport behavior in La-based perovskites: a density functional theory study. *The Journal of Physical Chemistry C* **123**, 275–290 (2018).
18. Curnan, M. T. & Kitchin, J. R. Effects of concentration, crystal structure, magnetism, and electronic structure method on first-principles oxygen vacancy formation energy trends in perovskites. *The Journal of Physical Chemistry C* **118**, 28776–28790 (2014).
19. Linderalv, C., Lindman, A. & Erhart, P. A unifying perspective on oxygen vacancies in wide band gap oxides. *J Phys Chem Lett* **9**, 222–228 (2018).

20. Muy, S. *et al.* Tuning mobility and stability of lithium ion conductors based on lattice dynamics. *Energy Environ Sci* **11**, 850–859 (2018).

21. Koehler, W. C. & Wollan, E. O. Neutron-diffraction study of the magnetic properties of perovskite-like compounds LaBO3. *Journal of Physics and Chemistry of Solids* **2**, 100–106 (1957).

22. Saitoh, T. *et al.* Electronic structure and temperature-induced paramagnetism in LaCoO 3. *Phys Rev B* **55**, 4257 (1997).

23. Kikuchi, J., Yasuoka, H., Kokubo, Y. & Ueda, Y. Antiferromagnetic Nuclear Resonance of 51V in LaVO3 and YVO3. *J Physical Soc Japan* **63**, 3577–3580 (1994).

24. Sreedhar, K. *et al.* Electronic properties of the metallic perovskite LaNiO 3: Correlated behavior of 3d electrons. *Phys Rev B* **46**, 6382 (1992).

25. Goral, J. P. & Greedan, J. E. The magnetic structures of LaTiO3 and CeTiO3. *J Magn Magn Mater* **37**, 315–321 (1983).

26. Wang, M. & Navrotsky, A. Enthalpy of formation of LiNiO2, LiCoO2 and their solid solution, LiNi1− xCoxO2. *Solid State Ion* **166**, 167–173 (2004).